

Supporting Information for
Multivariate Metal-Organic Framework MTV-MIL-101 via Post-Synthetic Cation Exchange: Is It Truly Applicable?

Mahmoud Y. Zorainy,^{a,b} Hatem M. Titi,^c Serge Kaliaguine,^d Daria. C. Boffito^{a*}

^a *Chemical Engineering Department, Polytechnique Montréal, Montréal, QC H3C 3A7 (Canada)*

^b *Chemical Engineering Department, Military Technical College, Cairo (Egypt)*

^c *Department of Chemistry, McGill University, Montréal, QC H3A 0B8 (Canada)*

^d *Chemical Engineering Department, Laval University, Québec, QC G1V 0A6 (Canada)*

**Corresponding Author: daria-camilla.boffito@polymtl.ca*

Table of Content	Page no.
1. Experimental details	S4
1.1 Materials	S4
1.2 Methods	S4
Synthesis of MIL-101(Cr)	S4
Synthesis of MIL-101(Fe)	S4
Post-synthetic cation-exchange	S5
2. Characterization	S6
3. Results	S8
Figure S1. Chemical stability investigation on the MIL-101(Fe) framework.	S8
Table S1. Application of the Post-synthetic modification (PSM) method on MIL-101(Cr) using aqueous solutions of FeCl ₃	S9
Table S2. Refluxing aqueous solutions of FeCl ₃ without the addition of MIL-101(Cr)	S10
Table S3. Application of the Post-synthetic modification (PSM) method on MIL-101(Cr) using aqueous solutions of Fe(NO ₃) ₃	S11

Table S4. Application of the Post-synthetic modification (PSM) method on MIL-101(Cr) using solutions of FeCl ₃ in DMF	S12
Table S5. Refluxing solutions of FeCl ₃ in DMF without the addition of MIL-101(Cr)	S13
Figure S2. PSE samples before drying, showing different color each.	S14
Figure S2. PSE samples before drying, showing different color each.	S15
4. Other results	S16
a- PXRD	S16
Figure S3. XRD patterns of MIL-101 before and after reflux.	S16
Figure S4. XRD patterns of the PSM-Cl samples refluxed without adding the MOF.	S17
Figure S5. XRD patterns of the PSM-DMF samples in the $2\theta = 3^\circ - 40^\circ$ range.	S17
Figure S6. XRD patterns of the PSM-DMF samples refluxed without adding the MOF.	S18
b- UV-Vis DRS	S19
Figure S7. UV-Vis spectrum of the PSM-10-Cl in comparison with the as-synthesized MIL-101(Cr) and MIL-101(Fe).	S19
c- FTIR	S20
Figure S8. FTIR spectra of the as-synthesized MIL-101(Cr), MIL-101(Fe), and the PSM-10-Cl sample.	S20
Figure S9. FTIR spectra of the PSM samples in aqueous solutions.	S21
Figure S10. FTIR spectra of the PSM-DMF samples.	S21
d- XRF	S22
Table S6. Elemental composition of all samples after the PSE process	S22
e-Raman	S23
Table S7. Raman microscope images of PSM-Cl samples at different magnifications.	S23
Figure S11. Spot analysis of different regions within sample PSM-100-Cl.	S26
Table S8. Raman microscope images of PSM-DMF samples at different magnifications	S27

f- SEM	S30
Figure S12. SEM image of the PSM-10-Cl sample with the mapping of the Cr and Fe distribution over the sample.	S30
Figure S13. SEM image of the PSM-25-Cl sample with its whole elemental mapping distribution over the sample.	S31
Figure S14. SEM image of the PSM-50-Cl sample with the mapping of the Cr and Fe distribution over the sample.	S32
Figure S15. SEM image of the PSM-50-Cl sample with its whole elemental mapping distribution over the sample.	S33
Figure S16. SEM image of the PSM-100-Cl sample with the mapping of the Cr and Fe distribution over the sample.	S34
Figure S17. SEM image of the PSM-100-Cl sample with its whole elemental mapping distribution over the sample.	S35
g- Nitrogen sorption	S36
Table S9. Specific surface area and pore volume of all PSM samples	S36
Figure S18. N ₂ sorption isotherms for pristine MIL-101(Cr), PSM-10-Cl, and PSM-10-DMF samples	S37
5. References	S38

1. Experimental details

All synthetic manipulations were performed under ambient atmosphere, unless otherwise stated.

1.1 Materials. Chromium(III) nitrate nonahydrate ($\text{Cr}(\text{NO}_3)_3 \cdot 9\text{H}_2\text{O}$, 99%), 1,4-Benzenedicarboxylic acid “terephthalic acid” (H_2BDC , 98%), Iron(III) chloride hexahydrate ($\text{FeCl}_3 \cdot 6\text{H}_2\text{O}$, 97%), Iron(III) nitrate nonahydrate ($\text{Fe}(\text{NO}_3)_3 \cdot 9\text{H}_2\text{O}$, 98%), and N,N-dimethyl formamide (anhydrous DMF, 99.8%) were purchased from Sigma-Aldrich, Canada. Acetone ($\geq 99.5\%$) and Ethanol (EtOH, 98%) were purchased from Fischer Scientific, USA.

All chemicals were used as received with no further processing. All glassware was washed with conc. HCl or aqua regia after each experiment to get rid of any metal oxide contamination present.

1.2 Methods.

- **Synthesis of MIL-101(Cr):** MIL-101(Cr) was synthesized hydrothermally following Bromberg’s method with slight modifications.[1]

The hydrothermal HF-free synthesis took place in a Parr’s 200-ml large capacity acid digestion vessel (Parr Instrument Company, Model# 4748A) to provide a sufficient MOF amount for the whole process of post-synthetic modification (PSM) and to ensure that all samples were from the same batch. First, 10 g $\text{Cr}(\text{NO}_3)_3 \cdot 9\text{H}_2\text{O}$ (25 mmol) and 4.15g H_2BDC (25 mmol) were mixed and added to 100 ml of deionized water. The solution was then stirred for 15 min resulting in a dark blue-colored suspension of a pH around 2.5. Next, the suspension was transferred into the Teflon-lined autoclave bomb and then heated to 218 °C in a conduction oven. The reaction was held at this temperature for 18 h without stirring. After this time, the bomb was left to cool down gradually to room temperature inside the oven over a period of 5-6 hrs.

The reaction yielded a sea green-colored suspension of a pH around 0.5. The powders were collected through centrifugation at a speed of 10,000 rpm for 10 min. The separated solids were then washed with water, ethanol, and DMF. Activation took place by keeping the MOF in DMF overnight at 75°C. After that, the activated MOF was washed with ethanol and acetone before drying at 60°C overnight.

- **Synthesis of MIL-101(Fe):** MIL-101(Fe) was synthesized via the microwave-assisted technique for the purposes of comparison. Following Metzler-Nolte’s findings, a diluted solution of iron(III) chloride and H_2BDC in DMF with a ratio of 1:1:565, respectively, would drive the reaction towards the formation of the MIL-101 phase.[2] In addition, with the metal ion in excess with respect to the organic linker, the MIL-101 phase would be predominant. The synthesis took place in a 30 ml glass vial of Anton Paar’s Monowave 400 microwave (MW) reactor. In a typical procedure, 0.675 g $\text{FeCl}_3 \cdot 6\text{H}_2\text{O}$ (2.45 mmol) and 0.206g H_2BDC (1.24 mmol) were directly

weighed into the reaction vials. Then, 15 ml DMF was added to the vial, and it was magnetically stirred for 30 min at room temperature until the complete dissolution of the precursors, resulting in a pale orange-colored solution. The vial was then covered with a Teflon-lined silicon septum and placed into the reaction chamber of the MW reactor. The reaction proceeded, holding a temperature of 150°C for 10 min under constant stirring (500 rpm). After the reaction, the synthesis vessel was cooled to room temperature by air circulation at 6 bar inside the MW reactor.

The reaction yielded an orange-colored suspension. The powders were collected through centrifugation at a speed of 10,000 rpm for 10 min. The separated solids were then washed with DMF and ethanol and then dried at 80°C.

- Post-synthetic cation exchange: Following Szilágyi's procedure, PSM of the activated MOF was achieved through the solvent-assisted cation substitution method (SACS).[3] In such a process, 100 mg MIL-101(Cr) was refluxed with 100 ml of $\text{FeCl}_3 \cdot 6\text{H}_2\text{O}$ aqueous solutions at 100°C for 72 h. The amount of $\text{FeCl}_3 \cdot 6\text{H}_2\text{O}$ in 100 ml deionized water was 10 mg for the initial experiments. Then, we increased the concentration to 25, 50, and 100 mg to probe the maximum achievable exchanged capacity. Samples were then centrifuged, washed with deionized water and ethanol. Drying took place at 85°C overnight. The process was repeated for a longer refluxing time of seven days. Besides, we also adopted $\text{Fe}(\text{NO}_3)_3 \cdot 9\text{H}_2\text{O}$ instead of the chloride to investigate the effect of a different precursor.

In addition to the process duration and the type of precursors, the reaction solvent was also varied. We selected DMF as a refluxing solvent adopting Kholdeeva's conditions for MIL-101(Fe) synthesis. 100 mg MIL-101(Cr) was refluxed with 100 ml DMF at the same concentration of $\text{FeCl}_3 \cdot 6\text{H}_2\text{O}$ (10 mg, 25 mg, 50 mg, and 100 mg). Then, the solution was kept for 24 h at 110°C. The same separation and washing steps were followed as before, whereby the products were centrifuged at 10,000 rpm for 10 min, then washed with DMF and ethanol. The samples were dried at 80°C overnight.

All samples were kept in a desiccator under vacuum until characterization.

2. Characterization.

Powder X-ray diffraction (PXRD) patterns were recorded on a Bruker D8 Advance X-ray diffractometer equipped with LYNXEYE linear position-sensitive detector (Bruker AXS, Madison, WI). Data was collected over a $2\theta = 3^\circ$ - 100° range at increments of 0.02° and a scanning rate of $0.2^\circ/\text{s}$. In the diffractometer, a $\text{Cu-K}\alpha$ source ($\lambda = 1.5406 \text{ \AA}$) was operated at a tube voltage and a current of 40 kV and 40 mA, respectively. Samples for PXRD were prepared by placing a thin layer of samples on a zero-background silicon crystal plate supported on a cup. For multiscan experiments to test MOF stability, we conducted 350 scans in which data was collected over a $2\theta = 3^\circ$ - 50° range at increments of 0.02° each for 12 min.

Fourier-transform Infrared (FTIR) spectra were collected using the Perkin Elmer 65 spectrophotometer equipped with an ATR diamond. With the high-efficiency ATR technique, a full range scan (4000 cm^{-1} - 450 cm^{-1}) was performed with a resolution of 4 cm^{-1} , and the data were averaged over 32 scans.

UV-Vis spectra were collected using a Thermo Scientific Evolution 220 UV-Vis spectrophotometer equipped with the integrated sphere accessory for powder samples diffuse reflectance measurements. A full wavelength scan (220 nm - 1100nm) was performed on all samples. The blank sample holder covered with Spectralon[®] was used as the reference. 50 mg of each sample was weighed into the equivalent sample holder with a spring to press the sample powders homogeneously. All samples were measured in the specular excluded (SPEX) mode with the sample holder window to be in direct contact with the walls of the integration sphere. The embedded Kubelka-Munk setting was used to convert reflectance measurements into equivalent absorption spectra.

X-ray fluorescence analysis (XRF, Benchtop Epsilon 4 - Malvern Panalytical) was employed to detect the elemental composition of all samples. Cr and Fe were the elements specified to be detected, and results were given in the normalized elemental percentage. For each sample, 100 mg was weighed into the 35-mm P1 cup assembled with the circular Mylar film of $3.5 \mu\text{m}$ thickness.

Raman spectra were obtained using a WITec alpha300R access confocal Raman microscope equipped with a motorized stage, CCD detector, and 1800 grooves/mm optical grating. In addition, the instrument was equipped with a green Co laser source of a 532 nm wavelength. Measurements were done using three collecting lenses (10x, 50x, and 100x). Powder samples were pressed against a glass microscope slide. Spot analysis was performed over some selected area in each sample with an accumulating response of 20 scans, each of a signal integration time of 10 s to differentiate between different phases included. Spectra were collected in the region from 100 cm^{-1} to 3500 cm^{-1} , with a resolution of 1 cm^{-1} . Besides, area analysis over a square area of a side length of $10 \mu\text{m}$ was also recorded to get a collective response for the whole sample. The laser power was in the range of 0.5 – 0.7 mW to avoid any local heating induced by the laser.

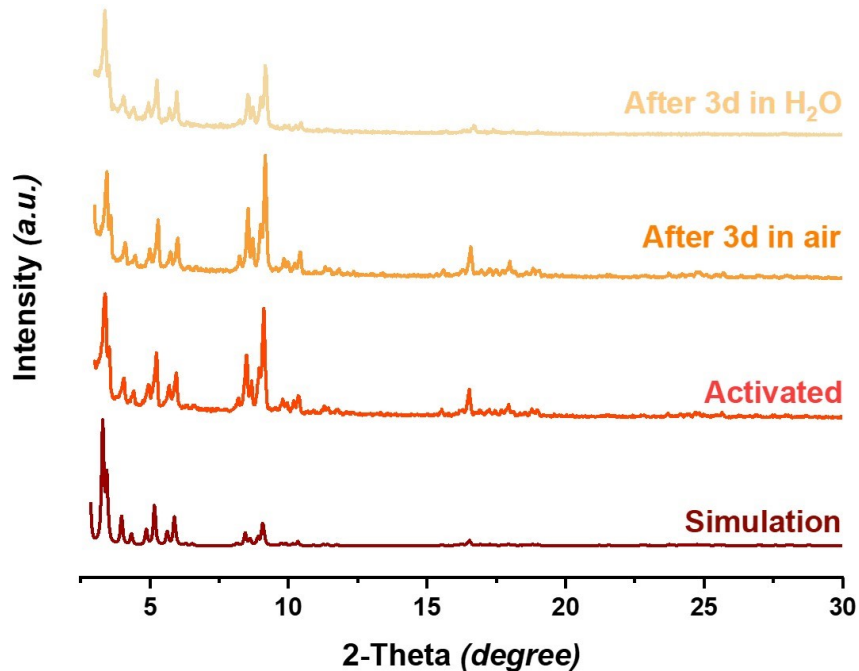
N_2 sorption experiments were carried out to measure the textural properties of the samples. Measurements took place at 77 K on the Autosorb iQ analyzer supplied from Quantachrome Instruments (USA). We used 100 mg of each sample. Sample outgassing took place at 170°C for 20 h under dynamic vacuum. Finally, the multi-point Brunauer-Emmett-Teller (BET) and the

Langmuir methods were applied to estimate all samples' specific surface area (S_{BET} , $S_{Langmuir}$) in the P/P_0 range ≤ 0.25 . On the other hand, the Barrett-Joyner-Hallender (BJH) and the Density-functional theory (DFT) calculations were used for the pore volume estimation at the point of $P/P_0 = 0.95$.

A scanning electron microscope (SEM, Benchtop Hitachi TM 3030 Plus) equipped with the energy-dispersive X-ray (EDX) detector screened the surface structure and the compositions of all the products. Samples were dispersed on double-sided carbon tape and mounted on an aluminum stub. Mainly, the instrument was operated on the back-scattered electron mode to distinguish between the different densities among the powders. A Carl Zeiss scanning electron microscope (Model: EVO MA 10, Germany) operated on the secondary electron mode was used to inspect the morphology of the obtained crystals at a higher magnification. The instrument detected the elements automatically, as well as their distribution and percentage abundance with respect to the mass ratio.

3. Results.

a)



b)

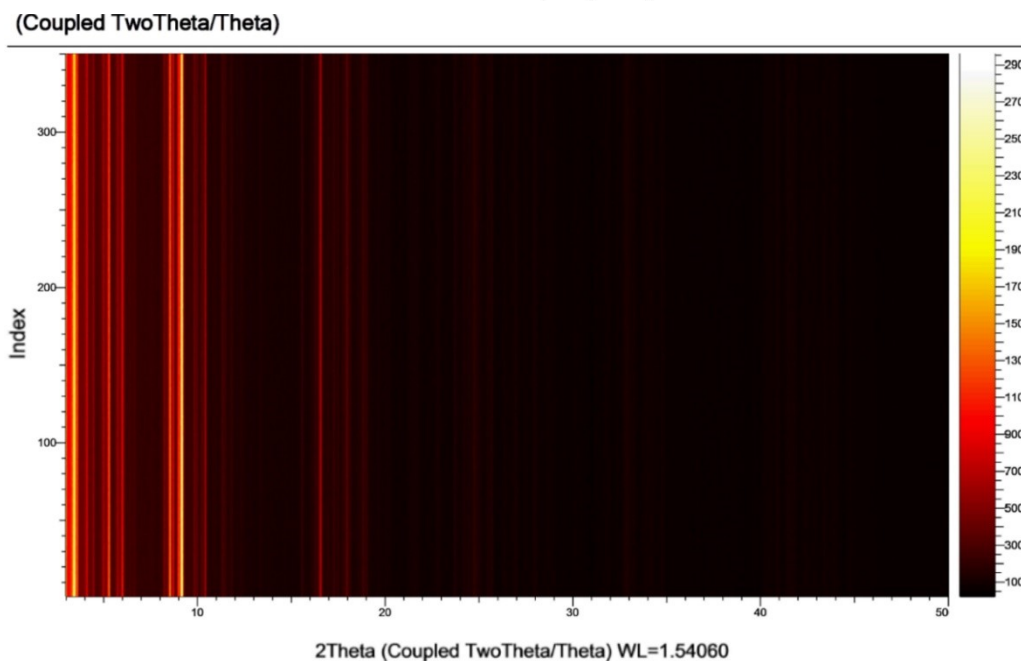


Figure S1. Chemical stability investigation on the MIL-101(Fe) framework. a) XRD patterns of the MIL-101(Fe) framework after prolonged exposure to air and water. (Maroon: Simulation “reproduced From CCDC file: OCUNAC”, Dark Orange: as-synthesized/ activated MIL-101(Fe), Light Orange: subjected to ambient atmosphere for 72 h, Beige: soaked in boiling water for 72 h). b) Two-dimensional XRD pattern for the MIL-101(Fe) sample after treatment with boiling water, followed by consecutive XRD stability scans for 72 h under air. Brighter lines indicate high-intensity accumulations at the corresponding 2θ.

Table S1. Application of the Post-synthetic modification (PSM) method on MIL-101(Cr) using aqueous solutions of FeCl₃

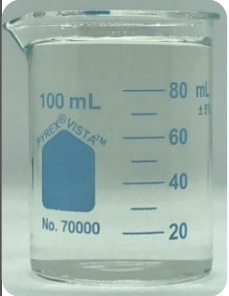
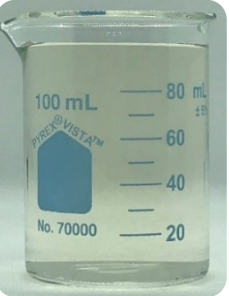
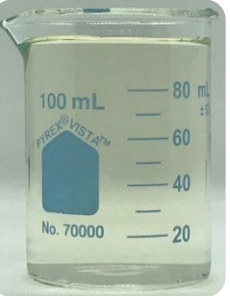
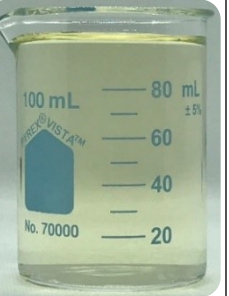
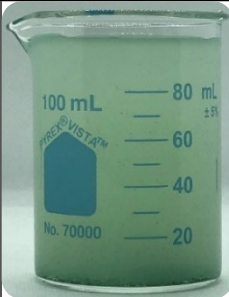


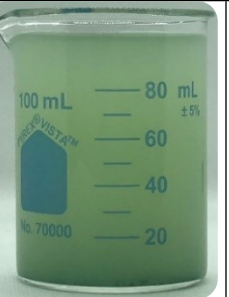
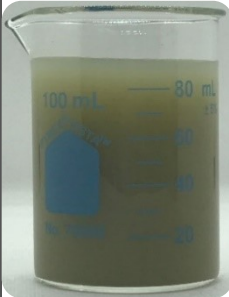






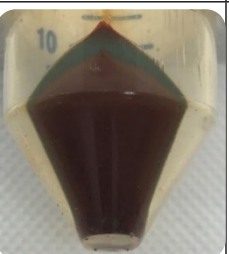
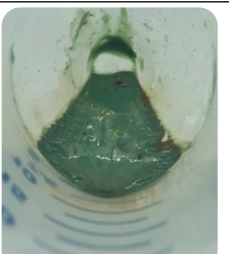






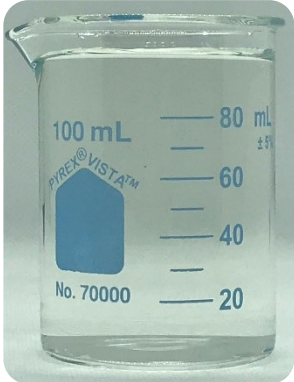
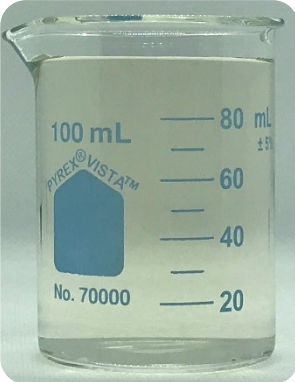
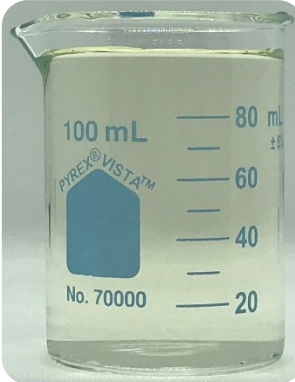
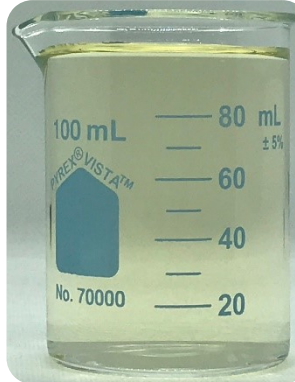
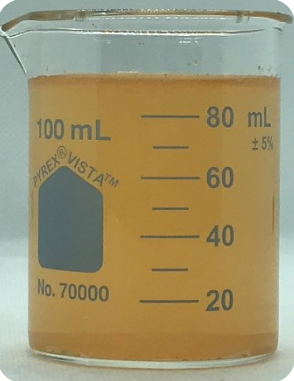
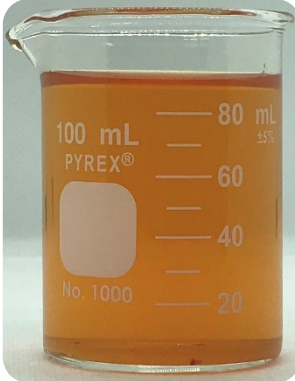

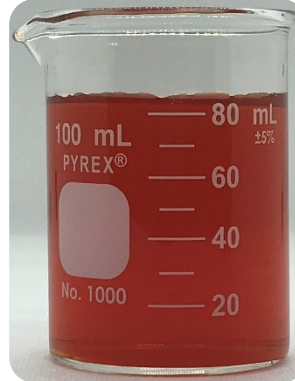


	10 mg FeCl ₃ (PSM-10)	25 mg FeCl ₃ (PSM-25)	50 mg FeCl ₃ (PSM-50)	100 mg FeCl ₃ (PSM-100)	Notes	
Aqueous Sol.					-----	
+ 100mg MOF					-----	
After reflux (72 h)					-----	
After Washing						Top view of the centrifuge tube
After Drying					 MIL-101(Cr)	 MIL-101(Fe)

Table S2. Refluxing aqueous solutions of FeCl₃ without the addition of MIL-101(Cr)

	10 mg FeCl ₃	25 mg FeCl ₃	50 mg FeCl ₃	100 mg FeCl ₃
Aqueous Sol.				
After reflux (72 h) No MOF				
After Drying	-----	-----		

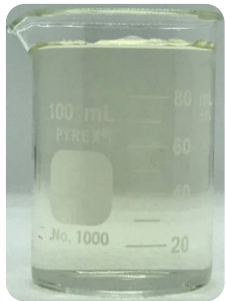
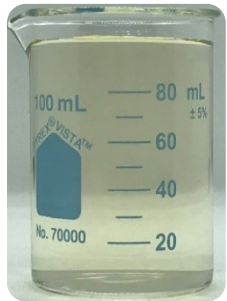






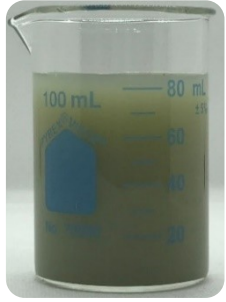
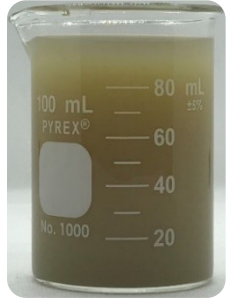
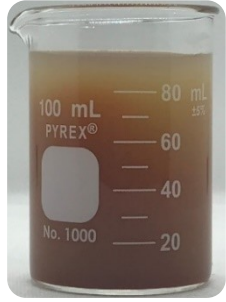










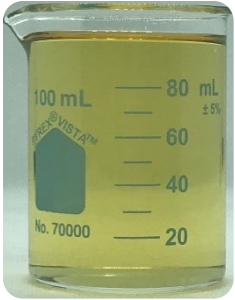
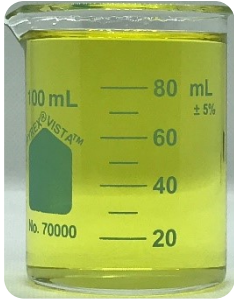

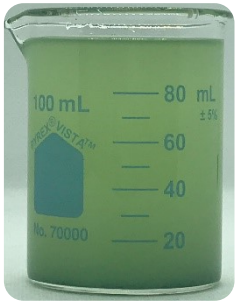
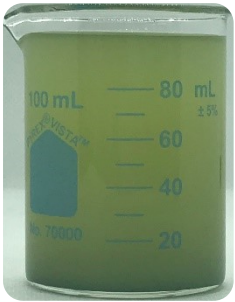



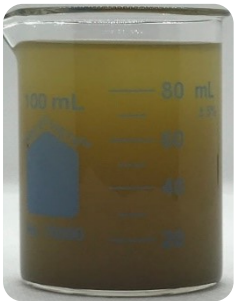
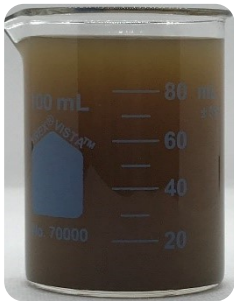

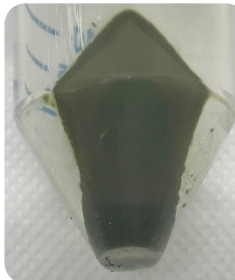



	10 mg Fe(NO ₃) ₃	25 mg Fe(NO ₃) ₃	50 mg Fe(NO ₃) ₃	100 mg Fe(NO ₃) ₃
Aqueous Sol.				
+ 100mg MOF				
After reflux (72 h)				
After Washing				
After Drying				

Table S3. Application of the Post-synthetic modification (PSM) method on MIL-101(Cr) using aqueous

	10 mg FeCl ₃	25 mg FeCl ₃	50 mg FeCl ₃	100 mg FeCl ₃
Solution in DMF				
+ 100mg MOF				
After reflux (24 h)				
After Washing				

solutions of Fe(NO₃)₃

Table S4. Application of the Post-synthetic modification (PSM) method on MIL-101(Cr) using solutions of FeCl₃ in DMF





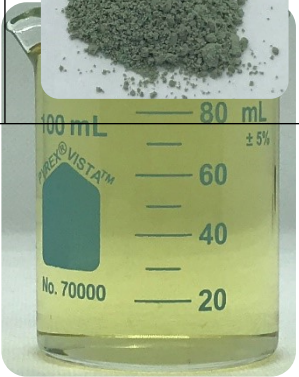
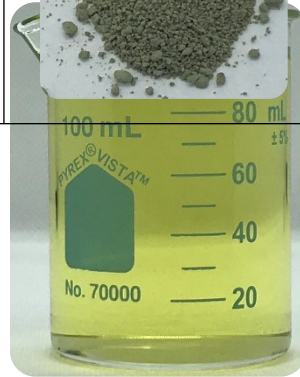



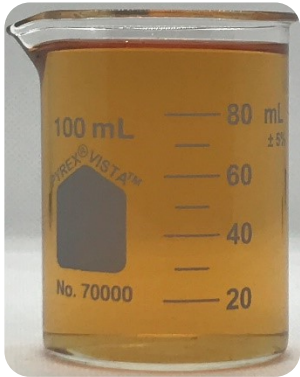
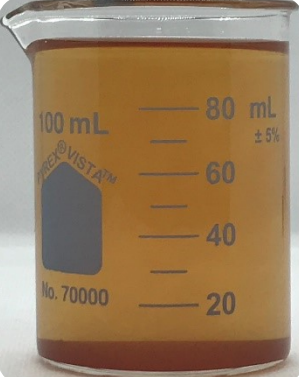



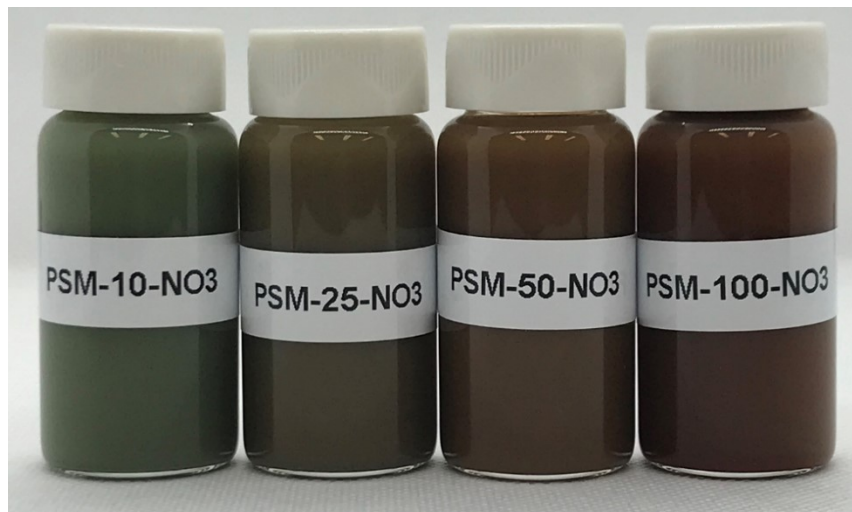
After Drying				
Solution in DMF				
After reflux (24 h) No MOF				
After Drying	-----	-----		

Table S5. Refluxing solutions of FeCl_3 in DMF without the addition of MIL-101(Cr)

a)



b)



c)

Figure S2. PSE samples before drying, showing a different color each. a) PSM-Cl samples. b) PSM-NO₃ samples. c) PSM-DMF samples.

a)



b)



c)

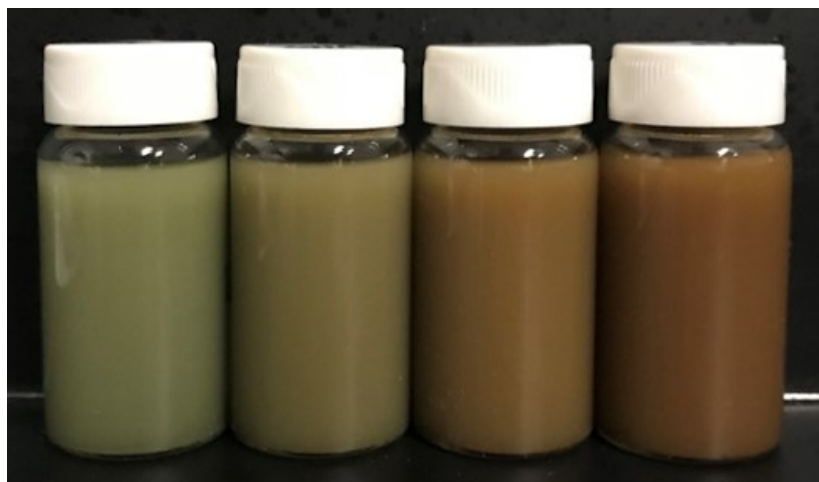


Figure S2. PSE samples before drying, showing a different color each. a) PSM-Cl samples. b) PSM-NO₃ samples. c) PSM-DMF samples.

4. Other results:

a- PXRD:

First, characterization via PXRD was performed to ensure the achievement of the MIL-101(Cr) framework by the HF-free method of Bromberg, whereby the resulting pattern (Fig. S1, “Red”) was very similar to the simulated one (Fig. S1, “Black”). Then, PXRD was applied to the obtained powders of the PSE method to ensure that the MIL-101 structure is still preserved with no transformation to any other framework isomer.

Starting with the 10 mg FeCl₃ sample (PSM-10-Cl), the pattern of this sample (Fig. S1, “Blue”) showed a nearly flat background, and all the high-intensity peaks were recognized in the $2\theta = 3^\circ - 10^\circ$ range. The pattern was very similar to that of the prepared MIL-101(Cr) with the main diffraction peaks at around $2\theta = 3.2^\circ, 3.9^\circ, 5.1^\circ, 5.8^\circ, 8.3^\circ,$ and 9.0° .

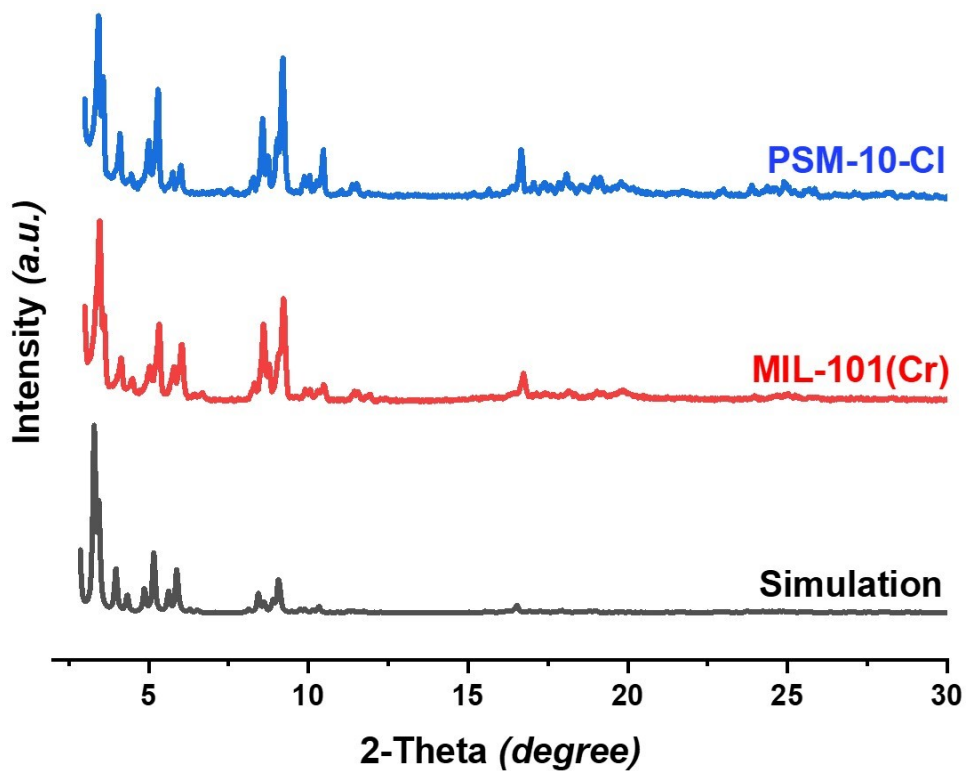


Figure S3. XRD patterns of the MIL-101(Cr) before and after reflux. (Black: Simulation “reproduced From CCDC file: OCUNAC”, Red: as-synthesized MIL-101(Cr), Blue: Products after refluxing with an aqueous sol. of 10 mg FeCl₃ for 72 h at 100°C.)

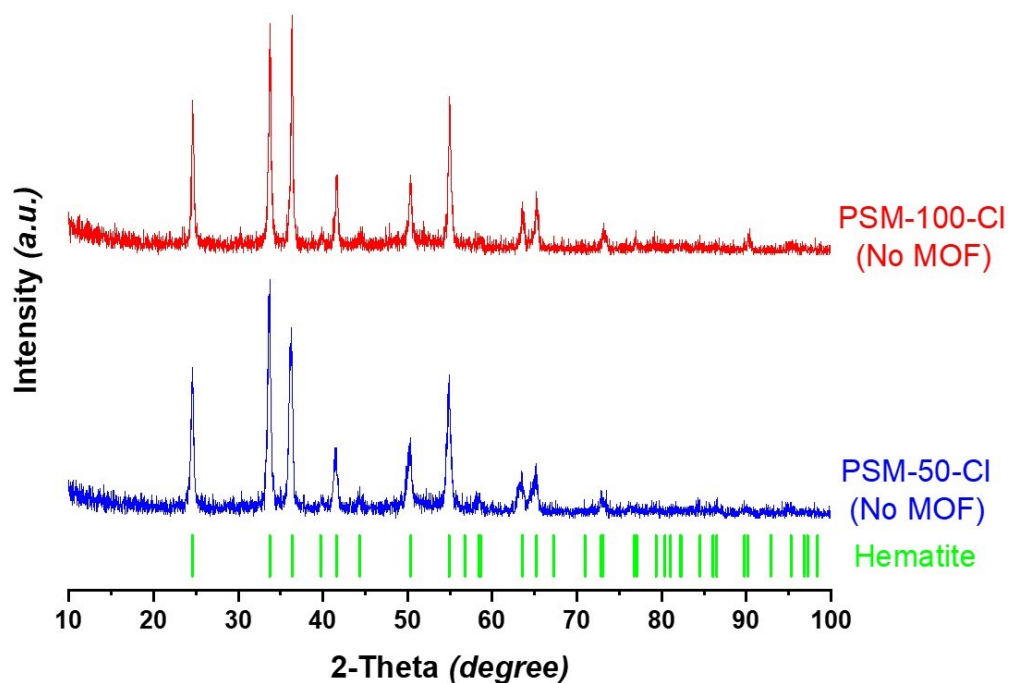


Figure S4. XRD patterns of the PSM-Cl control samples refluxed without adding the MOF compared to the diffraction peaks of hematite “light-green”.

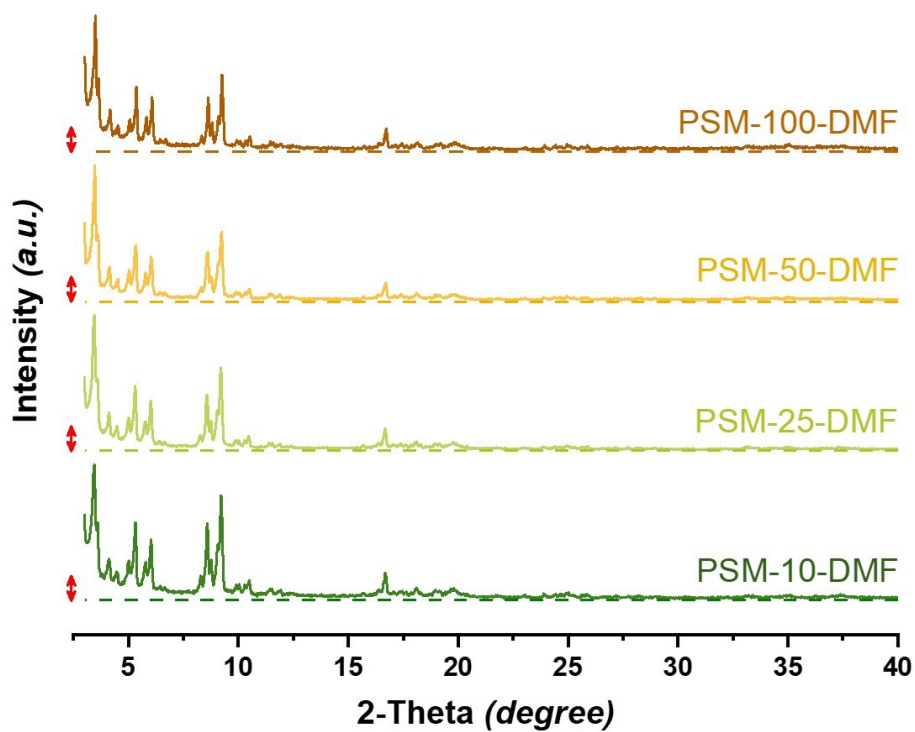


Figure S5. XRD patterns of the PSM-DMF samples in the $2\theta = 3^\circ - 40^\circ$ range (PSM-10-DMF “Dark green” to PSM-100-DMF “Brown”).

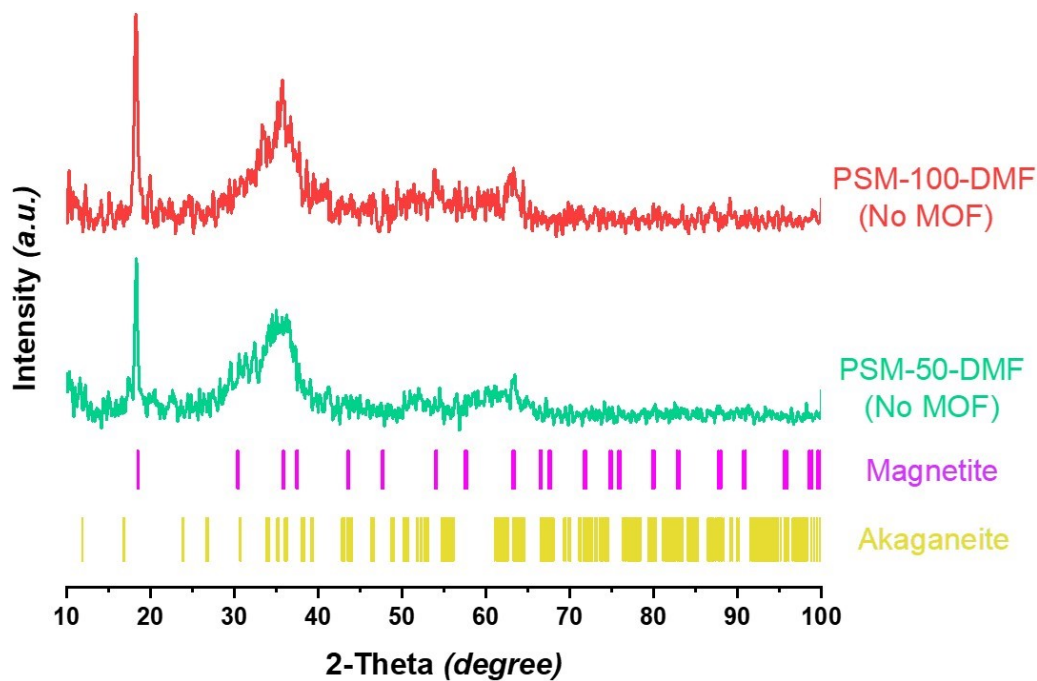


Figure S6. XRD patterns of the PSM-DMF control samples refluxed without adding the MOF compared to the diffraction peaks of magnetite “magenta” and akaganeite “yellow”.

b- UV-Vis DRS:

UV-Vis diffuse reflectance spectroscopy (DRS) is a sensitive characterization technique in the case of mixed-metal MOFs built from different 3d elements in their powder form.[3, 4] In such a technique, transition-metal MOFs show characteristic absorption in the visible range corresponding to the metals' d-d electrons excitation, which is the main reason for the various colors acquired by these MOFs based on their different metal centers. Thus, such a technique can be used to qualitatively detect the substitution of the structure's main metal constituent with other cations of similar nature.

The UV-Vis spectrum of MIL-101(Cr) showed three absorption bands in the UV and visible regions (Fig. S3). The absorption peak in the UV range around 288 nm results from the internal ligand π - π^* charge transition (ILCT). The other two peaks in the visible range around 439 nm and 593 nm are attributed to electronic transitions between the internal energy levels of Cr trimer, expressing its light sea-green color. On the other hand, the absorption bands of MIL-101(Fe) in the UV and visible range (220 nm - 600 nm) were convoluted showing a broad peak. However, a weak absorption could be witnessed around 957 nm within the near IR range.

The spectrum of the PSM-10-Cl sample was comparable to that of MIL-101(Cr), with its distinguishable absorption in the UV-Vis range and no other absorption at longer wavelengths. Nevertheless, the spectrum revealed a higher absorption in the visible and near UV range between 330 nm and 750 nm. In addition, the peak at around 439 nm showed some broadness compared to

the pristine sample, and the peak around 593 was slightly shifted (blue-shift) towards shorter wavelengths.

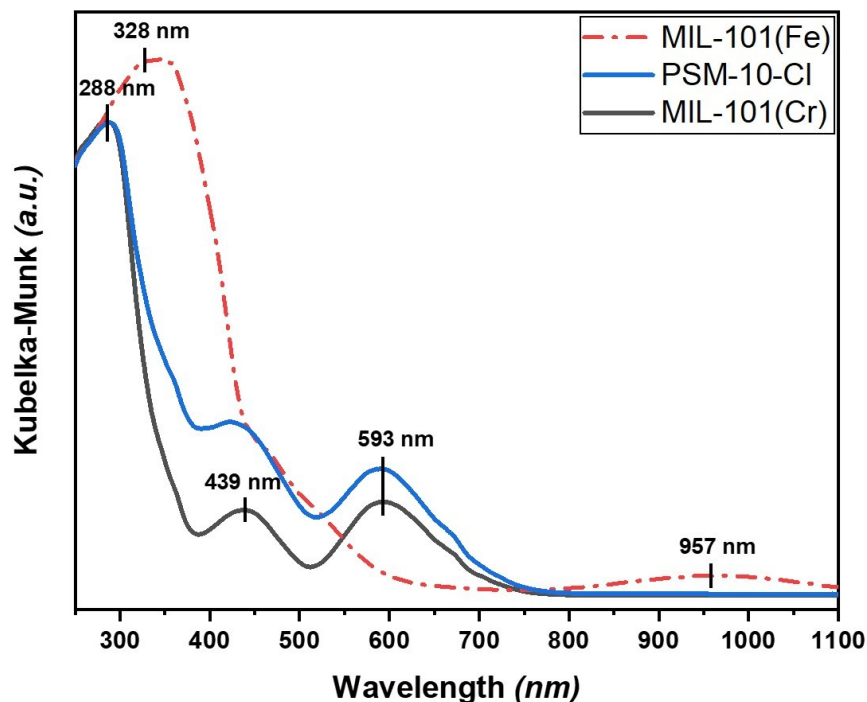


Figure S7. UV-Vis spectrum of the PSM-10-Cl (blue solid line) in comparison with the as-synthesized MIL-101(Cr) (black solid line) and MIL-101(Fe) (red dashed line).

c- FTIR:

FTIR was used to confirm that the composition of the MIL-101 structure is still maintained after reflux and the incorporation of Fe(III) into the structure through PSM. The vibrational spectrum of the 10 mg FeCl_3 sample (PSM-10-Cl) was almost typical to that of pristine MIL-101(Cr).[5-8] First, the vibrations of the carboxylate group bonds and the aromatic ring were recognized within the $1750\text{-}1250\text{ cm}^{-1}$ range. Peaks in the 1250 cm^{-1} to 600 cm^{-1} region are attributed to the C-H bonds of the ring. In the region below 600 cm^{-1} , the metal-O bonds' vibrations were detected.

The antisymmetric and symmetric stretching of the dicarboxylate groups matched the absorption bands at around 1631 cm^{-1} and 1398 cm^{-1} , respectively.[7, 9] The stretching of the aromatic ring (C=C) bonds was assigned to the peak at 1507 cm^{-1} .[5, 6, 10] In addition, the peaks at around 1017 cm^{-1} , 744 cm^{-1} , 1166 cm^{-1} , and 883 cm^{-1} are attributed to the in-plane and out-of-plane bending of the (C-H) bond.[5, 6, 8, 10] In both spectra of pristine MIL-101(Cr) and PSM-10-Cl, the Cr-O bonds' absorption could be detected at around 589 cm^{-1} .[5, 6] On the other hand, the spectrum of the PSM-10-Cl sample showed a recognizable shoulder at around 550 cm^{-1} matching with the Fe-O peak in pristine MIL-101(Fe).[6, 11, 12]

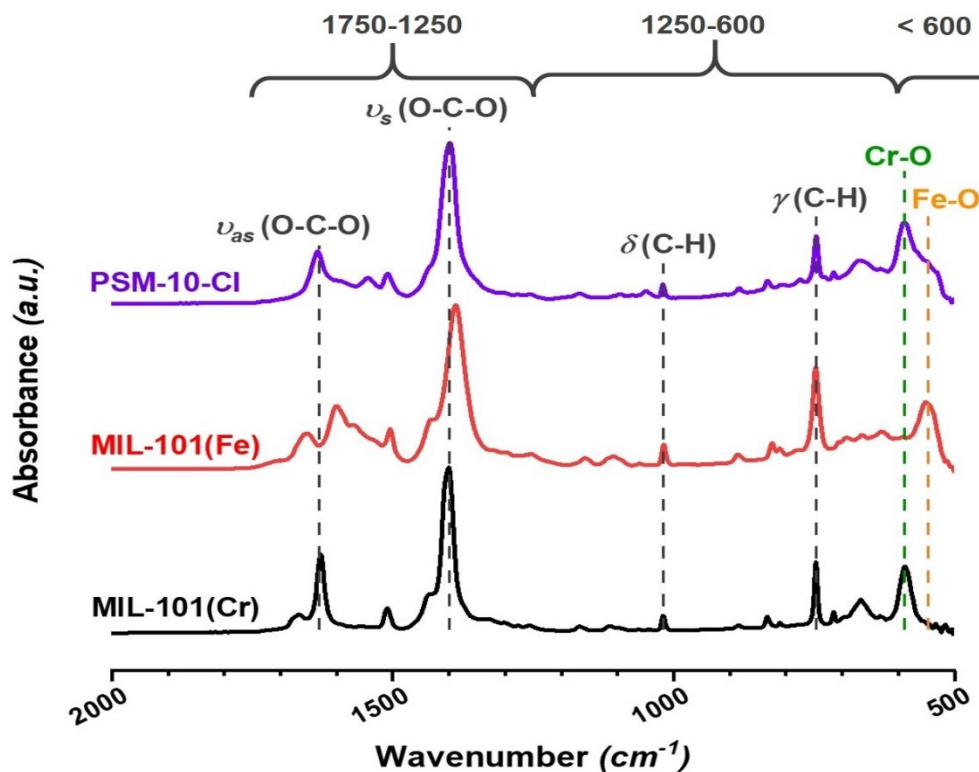


Figure S8. FTIR spectra of the as-synthesized MIL-101(Cr) (black) and MIL-101(Fe) (red) compared to that of the PSM-10-Cl sample (magenta), showing the shoulder at around 550 cm^{-1} , corresponding to the Fe-O bond vibrations.

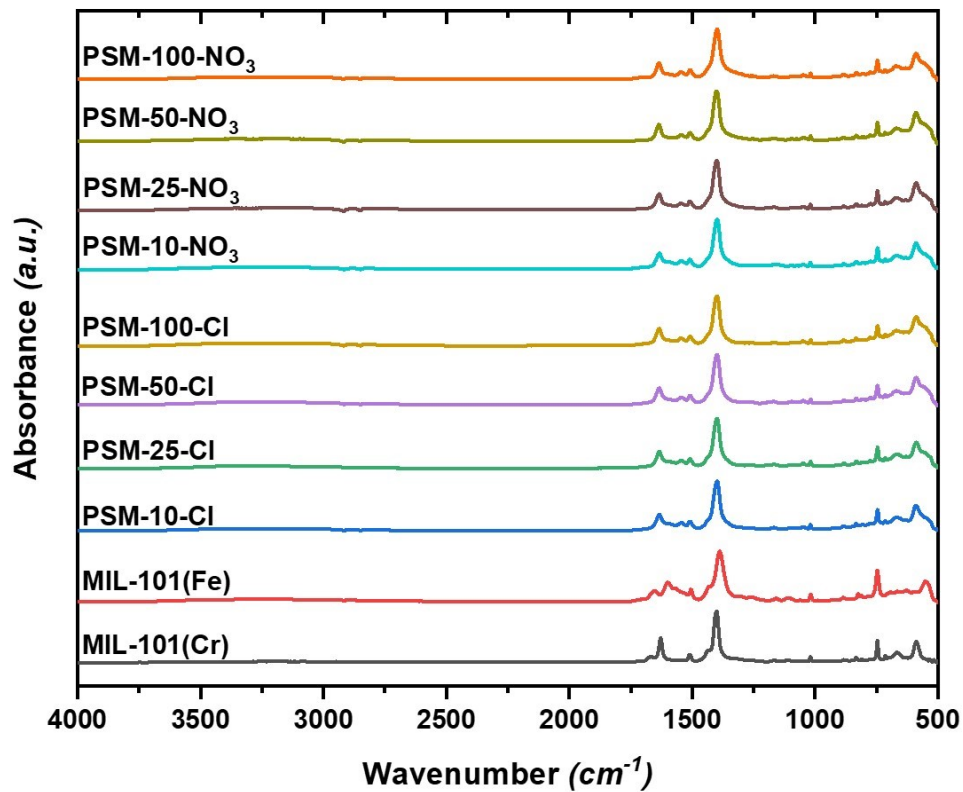


Figure S9. FTIR spectra of the PSM samples in aqueous solutions.

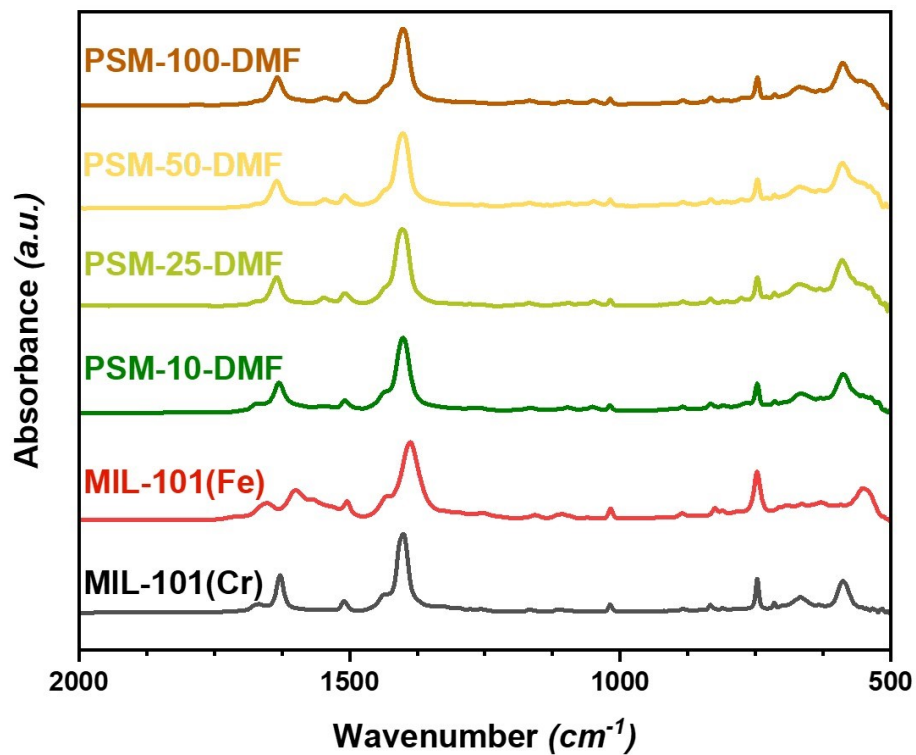


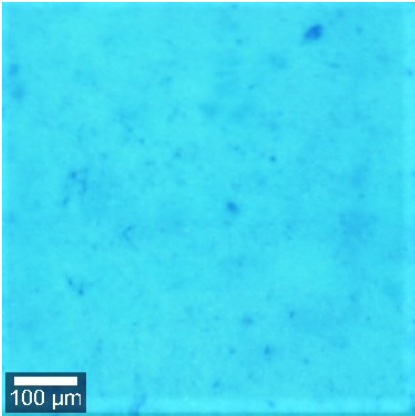
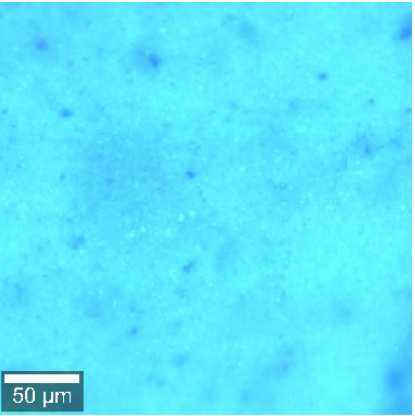
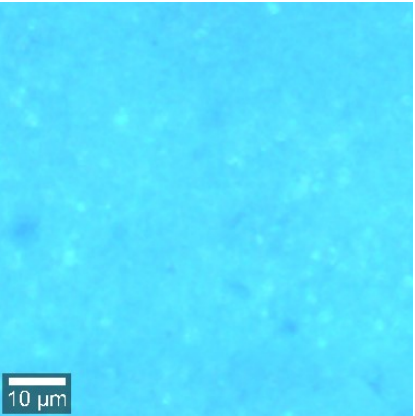
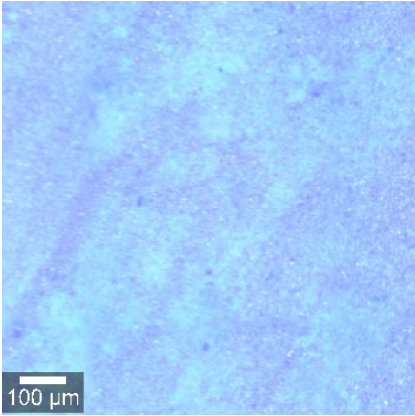
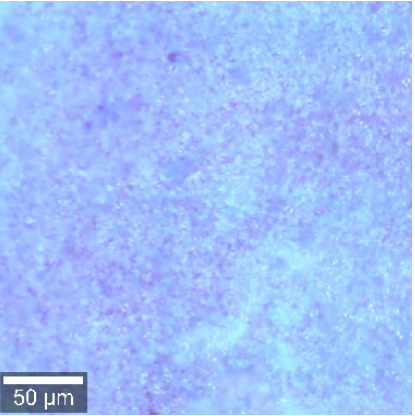
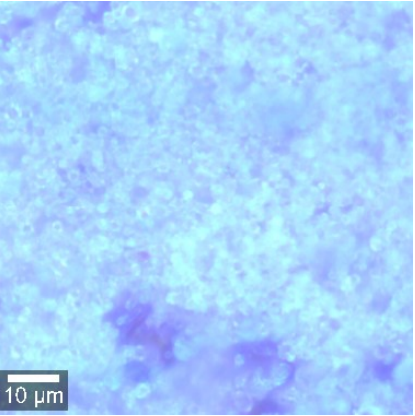
Figure S10. FTIR spectra of the PSM-DMF samples.

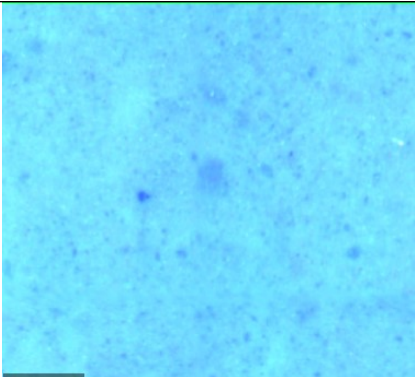
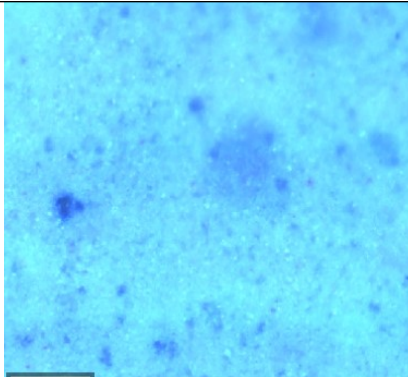
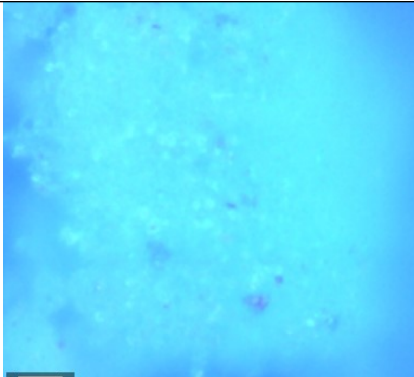
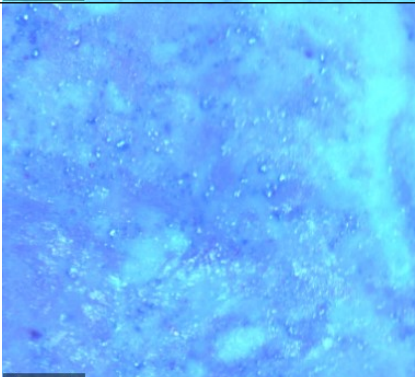
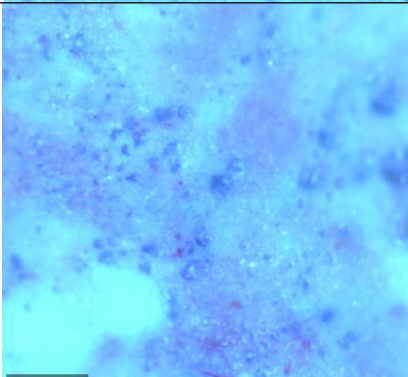
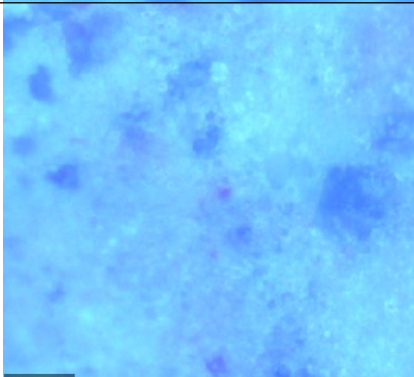
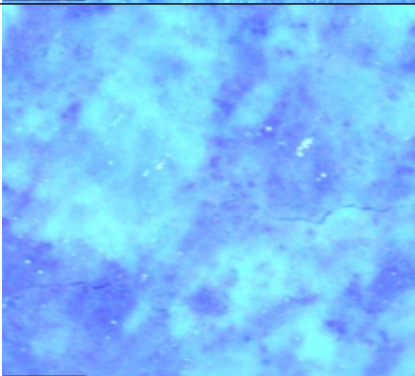
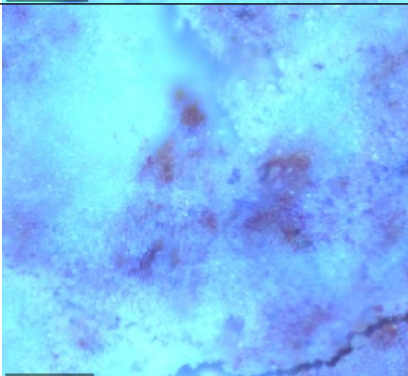
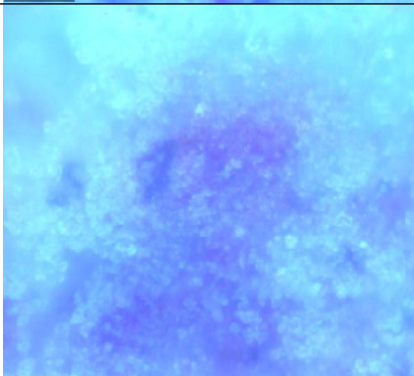
Sample	PSM-0-Cl		PSM-10-Cl		PSM-25-Cl		PSM-50-Cl		PSM-100-Cl	
Technique	XRF	SEM	XRF	SEM	XRF	SEM	XRF	SEM	XRF	SEM
Cr	99.9	99.9	82.9	85.9	71.1	76.8	55.8	59.5	43.9	46.4
Fe	0.1	0.1	17.1	14.1	28.9	23.2	44.2	40.5	56.1	53.6
Sample	PSM-0-Cl		PSM-10-NO3		PSM-25-NO3		PSM-50-NO3		PSM-100-NO3	
Technique	XRF	SEM	XRF	SEM	XRF	SEM	XRF	SEM	XRF	SEM
Cr	99.9	99.9	86.6	88.8	75.2	78.1	54.7	58.3	43.9	47.1
Fe	0.1	0.1	13.4	11.2	24.8	21.9	45.3	41.7	56.1	52.9
Sample	PSM-0-DMF		PSM-10-DMF		PSM-25-DMF		PSM-50-DMF		PSM-100-DMF	
Technique	XRF	SEM	XRF	SEM	XRF	SEM	XRF	SEM	XRF	SEM
Cr	99.9	99.9	81.1	82.4	68.2	69.6	53.2	54.9	39.3	41.8
Fe	0.1	0.1	18.9	17.6	31.8	30.4	46.8	45.1	60.7	58.2

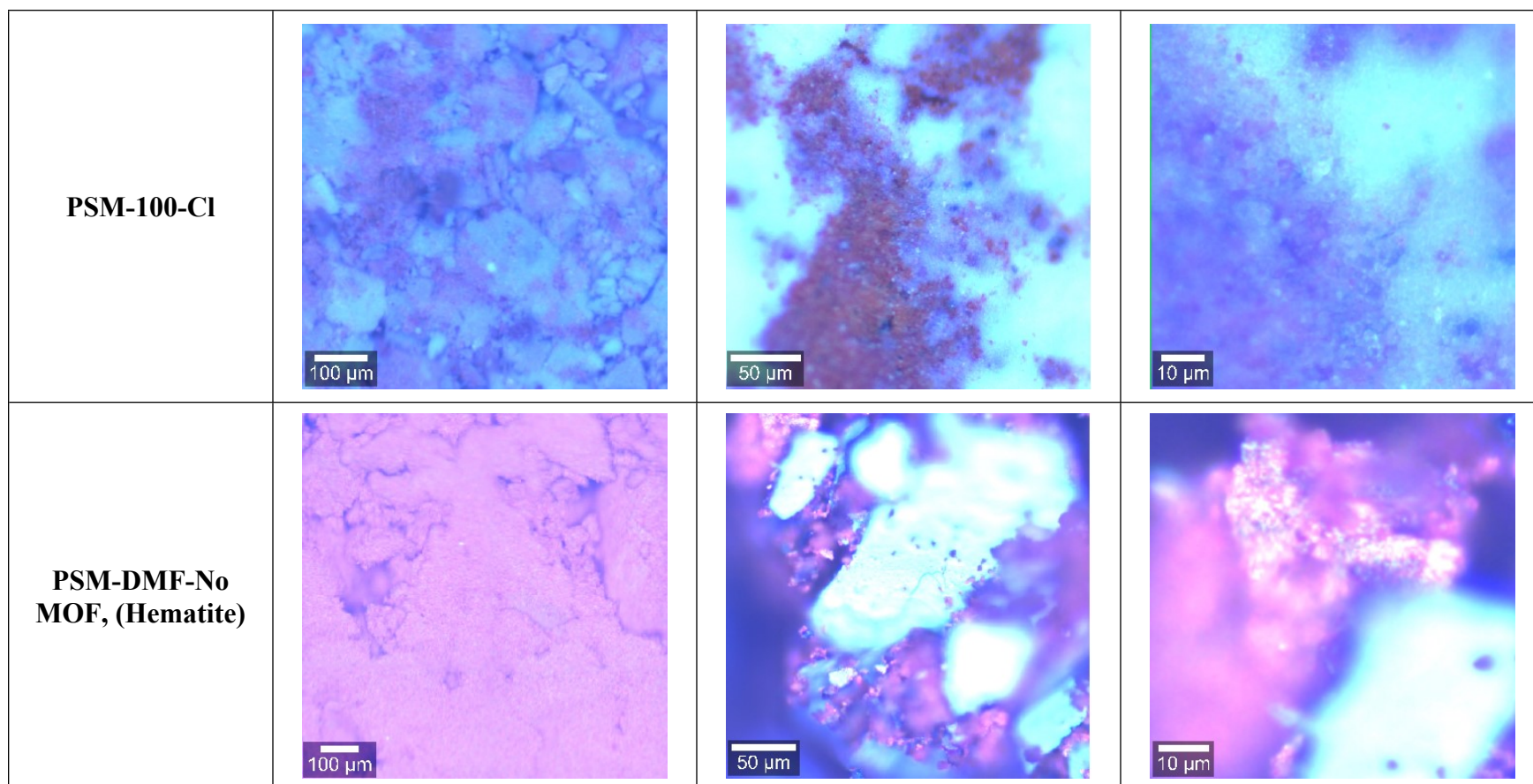
Table S6. Elemental composition of all samples after the PSE process

e- Raman

Table S7. Raman microscope images of PSM-CI samples at different magnifications

<i>Magnification</i> <i>Sample</i>	<i>10x</i>	<i>50x</i>	<i>100x</i>
MIL-101(Cr)			
MIL-101(Fe)			

PSM-10-C1	 100 μm	 50 μm	 10 μm
PSM-25-C1	 100 μm	 50 μm	 10 μm
PSM-50-C1	 100 μm	 50 μm	 10 μm



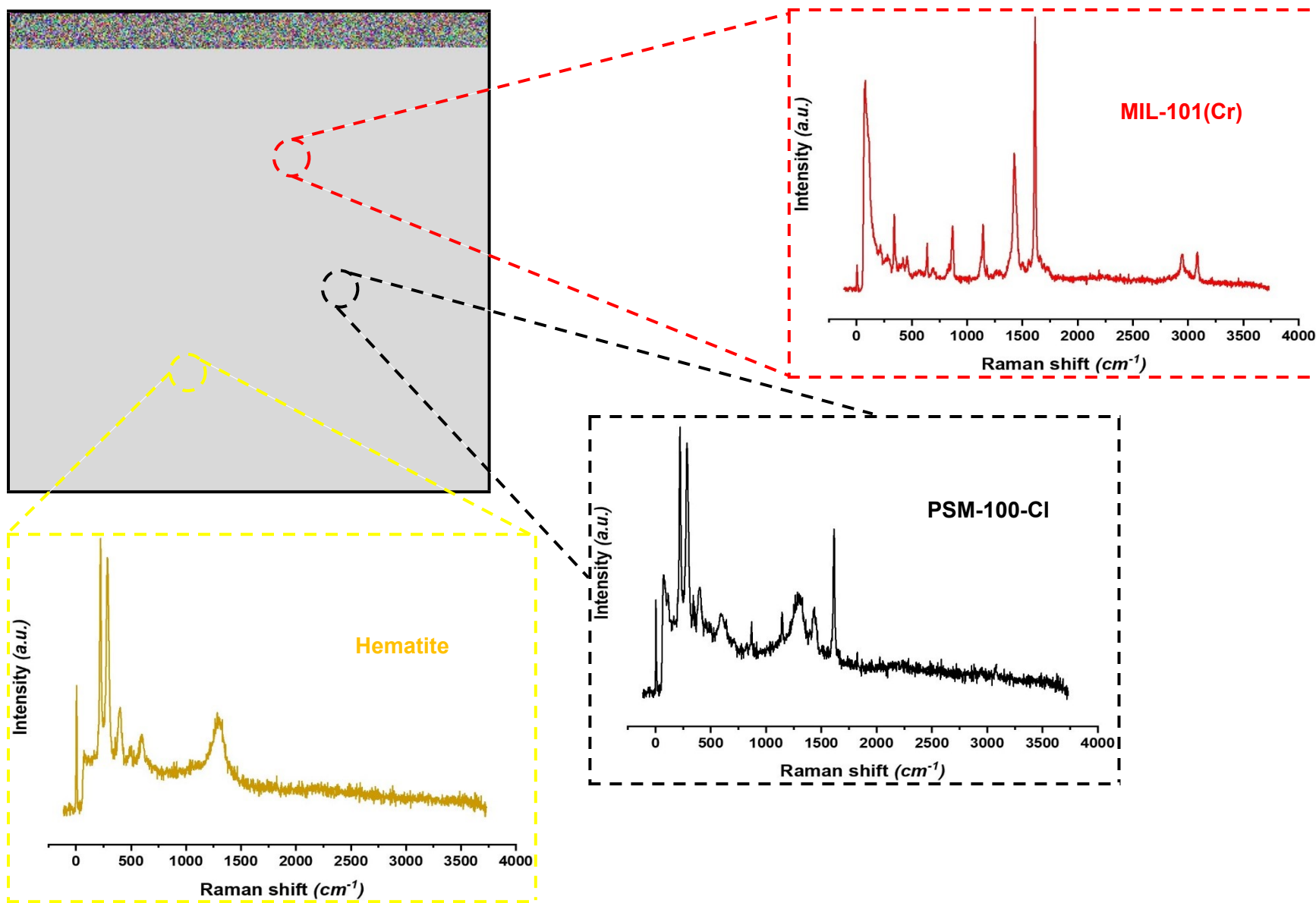
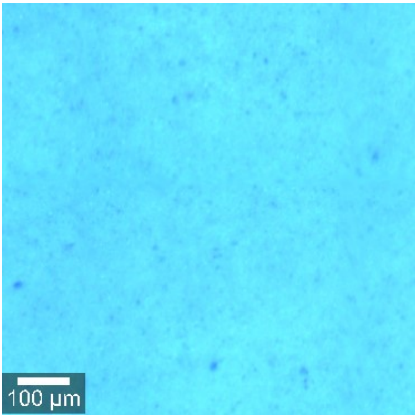
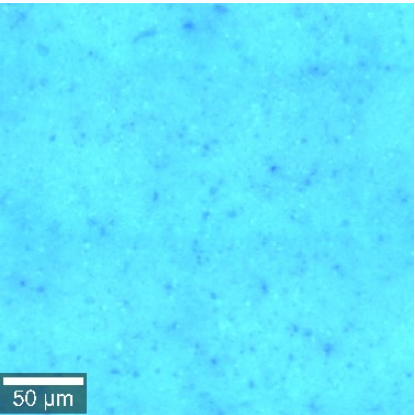
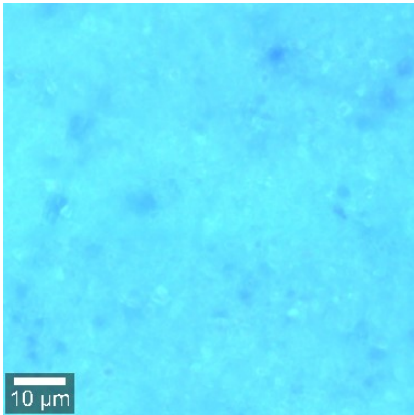
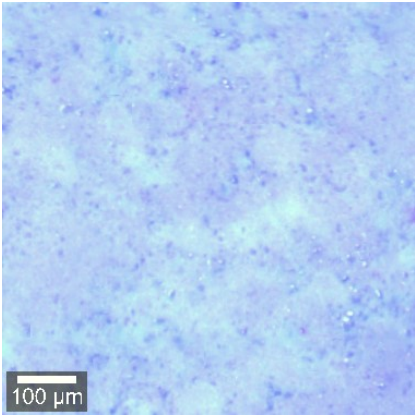
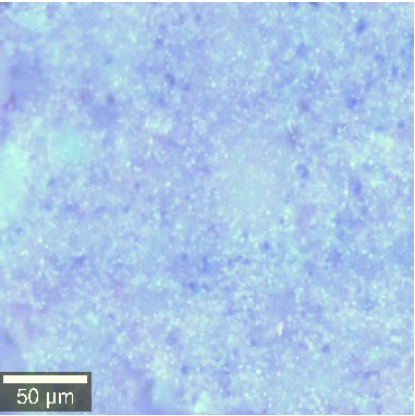
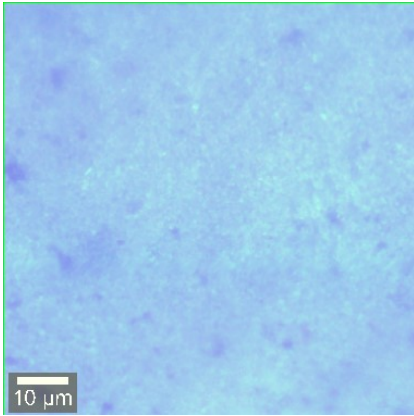
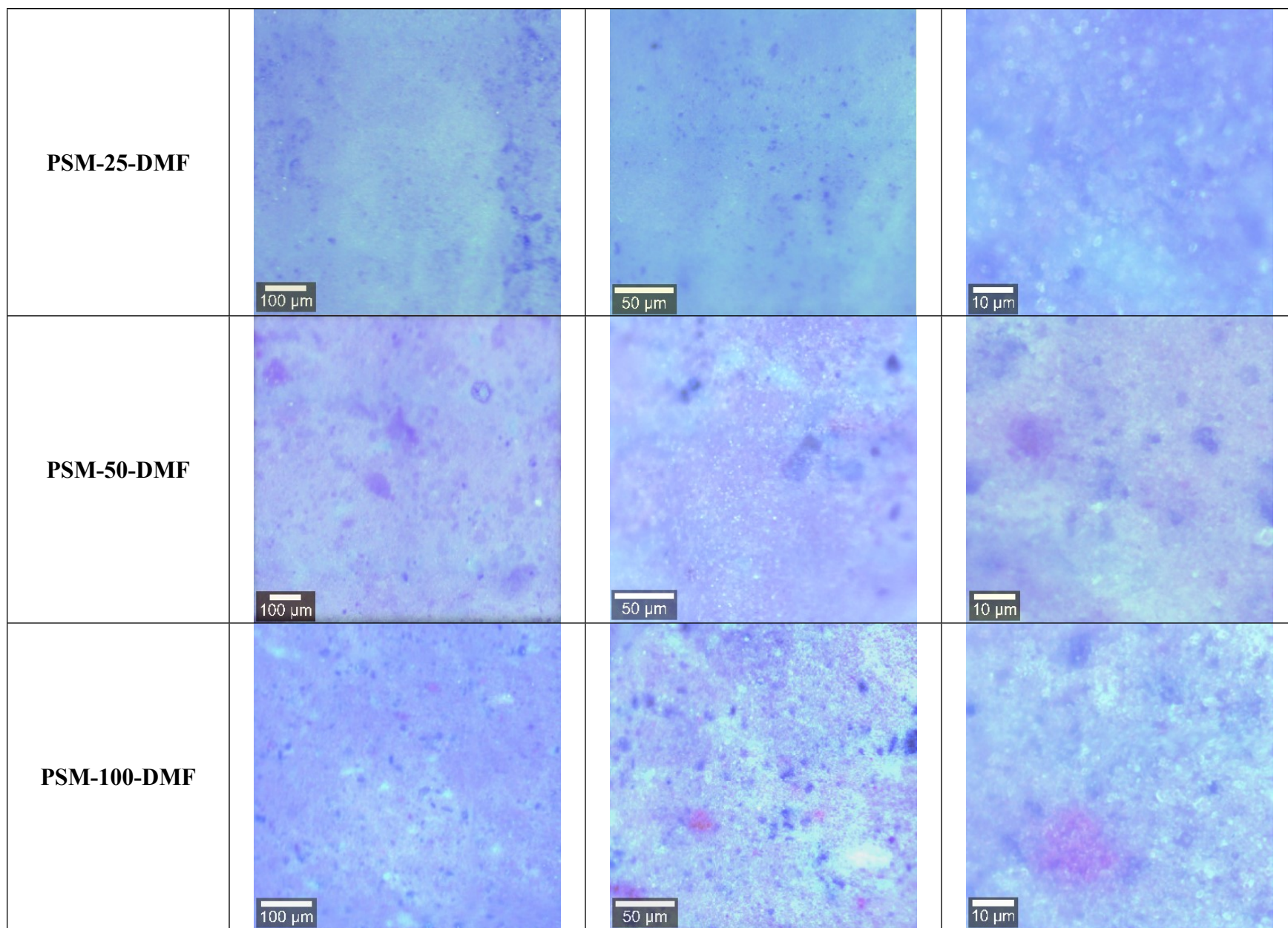


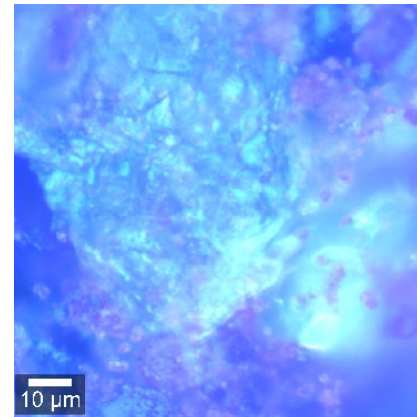
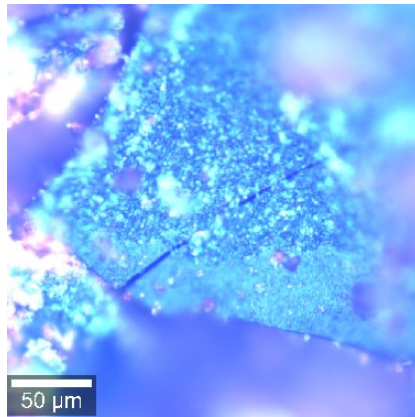
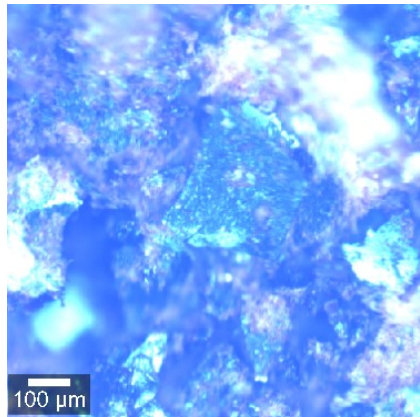
Figure S11. Spot analysis of different regions within sample PSM-100-Cl.

Table S8. Raman microscope images of PSM-DMF samples at different magnifications

<i>Magnification</i> <i>Sample</i>	<i>10x</i>	<i>50x</i>	<i>100x</i>
PSM-0-DMF			
PSM-10-DMF			



**PSM-DMF-No
MOF**



f- SEM

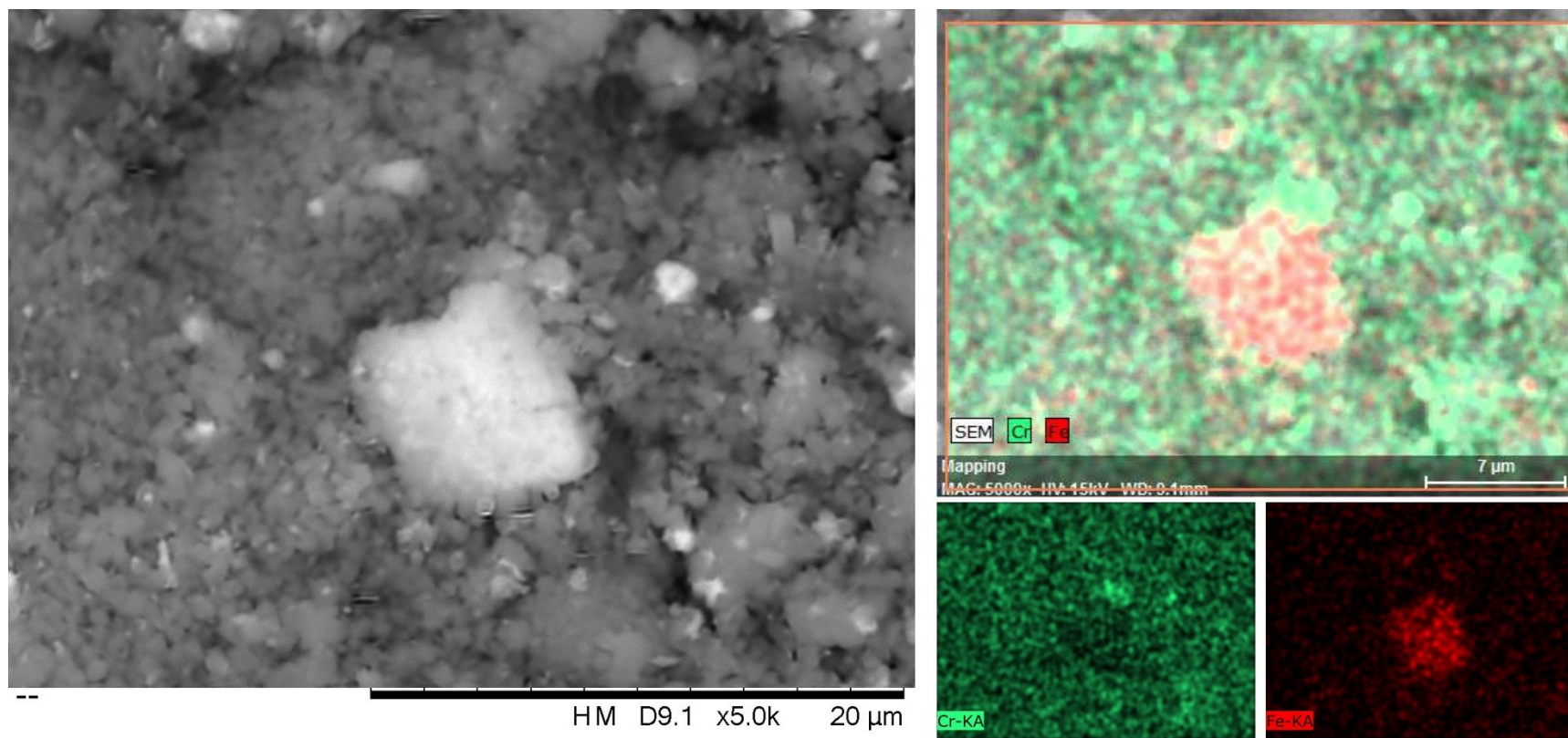


Figure S12. SEM image of the PSM-25-C1 sample with the mapping of the Cr and Fe distribution over the sample.

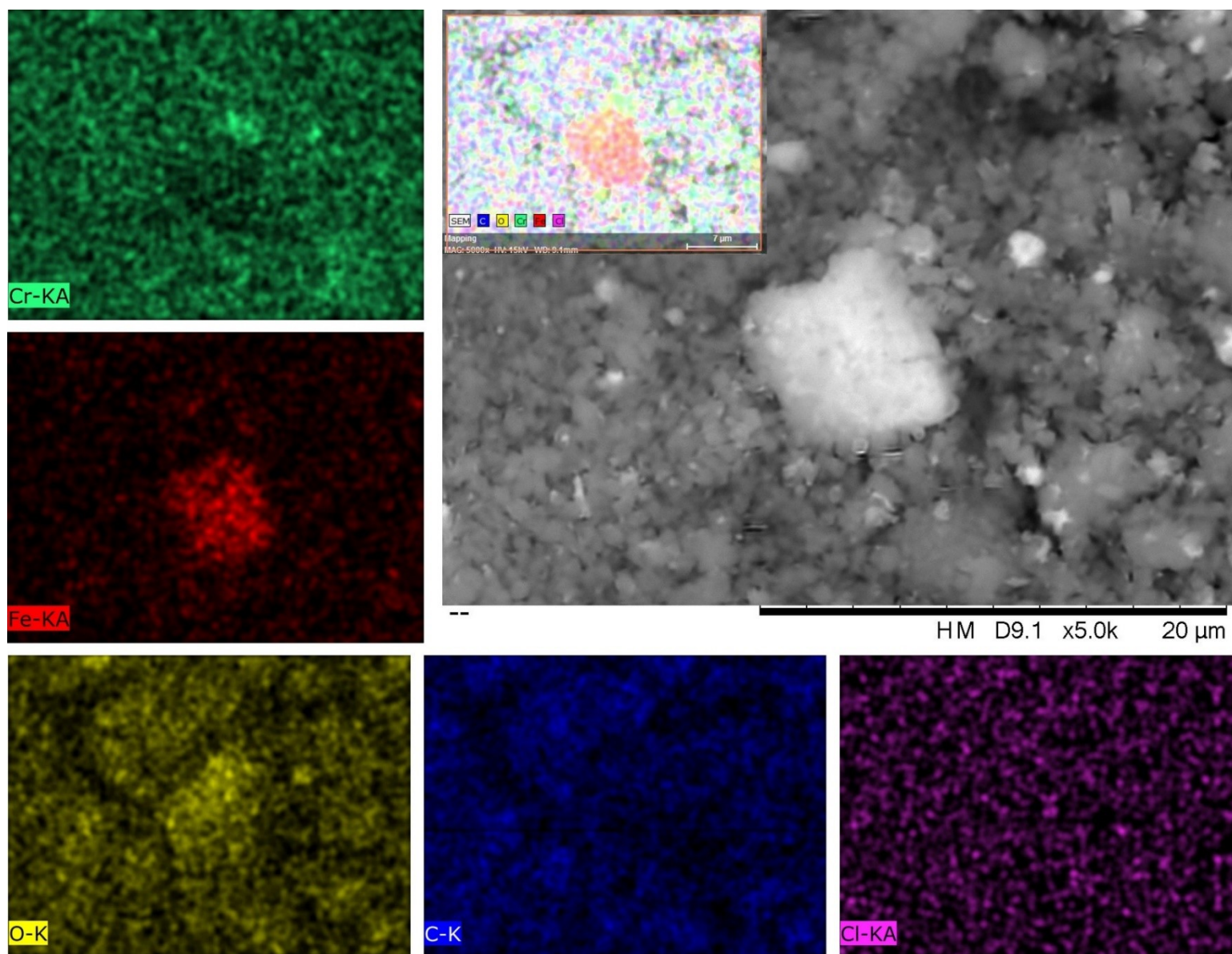


Figure S13. SEM image of the PSM-25-Cl sample with its whole elemental mapping distribution over the sample

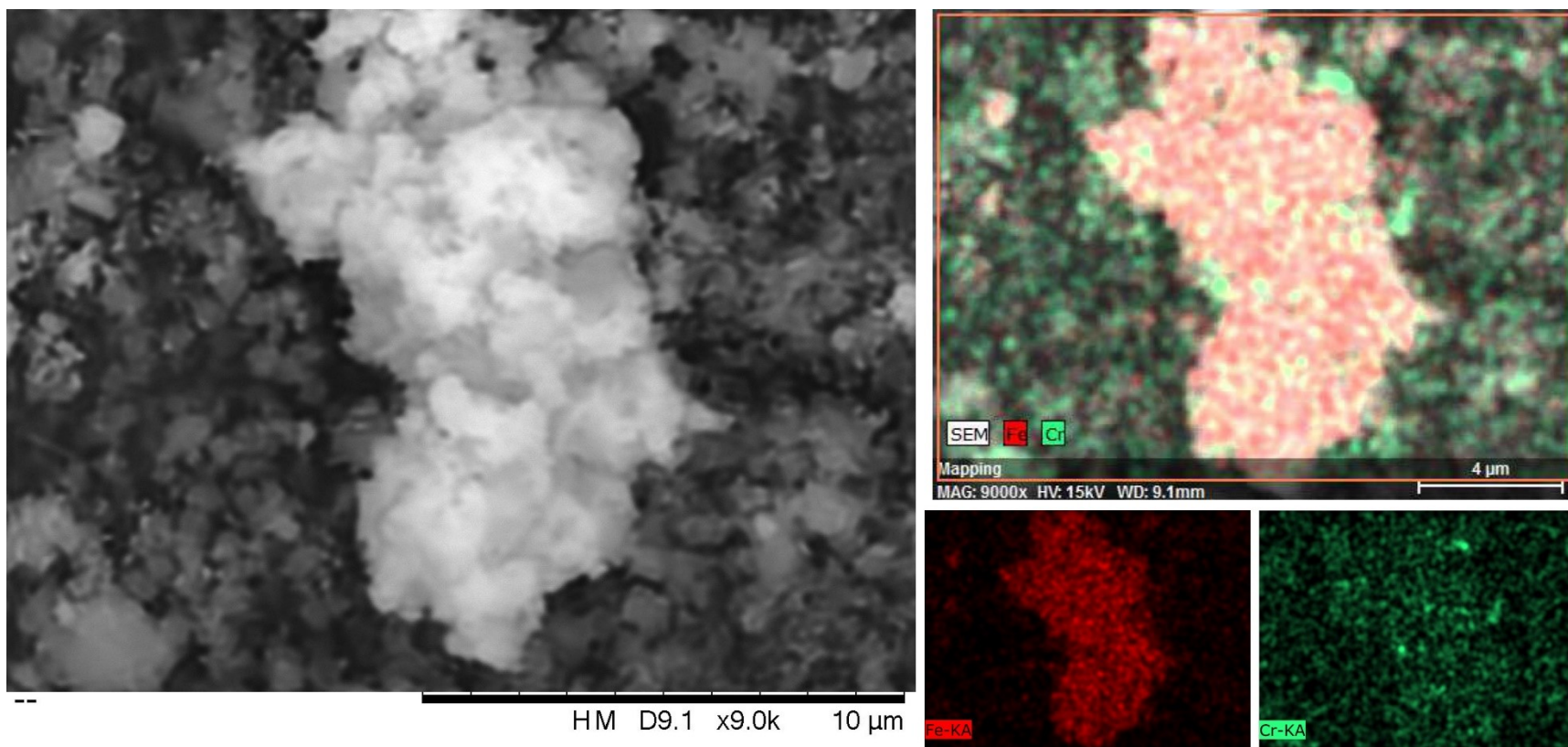


Figure S14. SEM image of the PSM-50-C1 sample with the mapping of the Cr and Fe distribution over the sample.

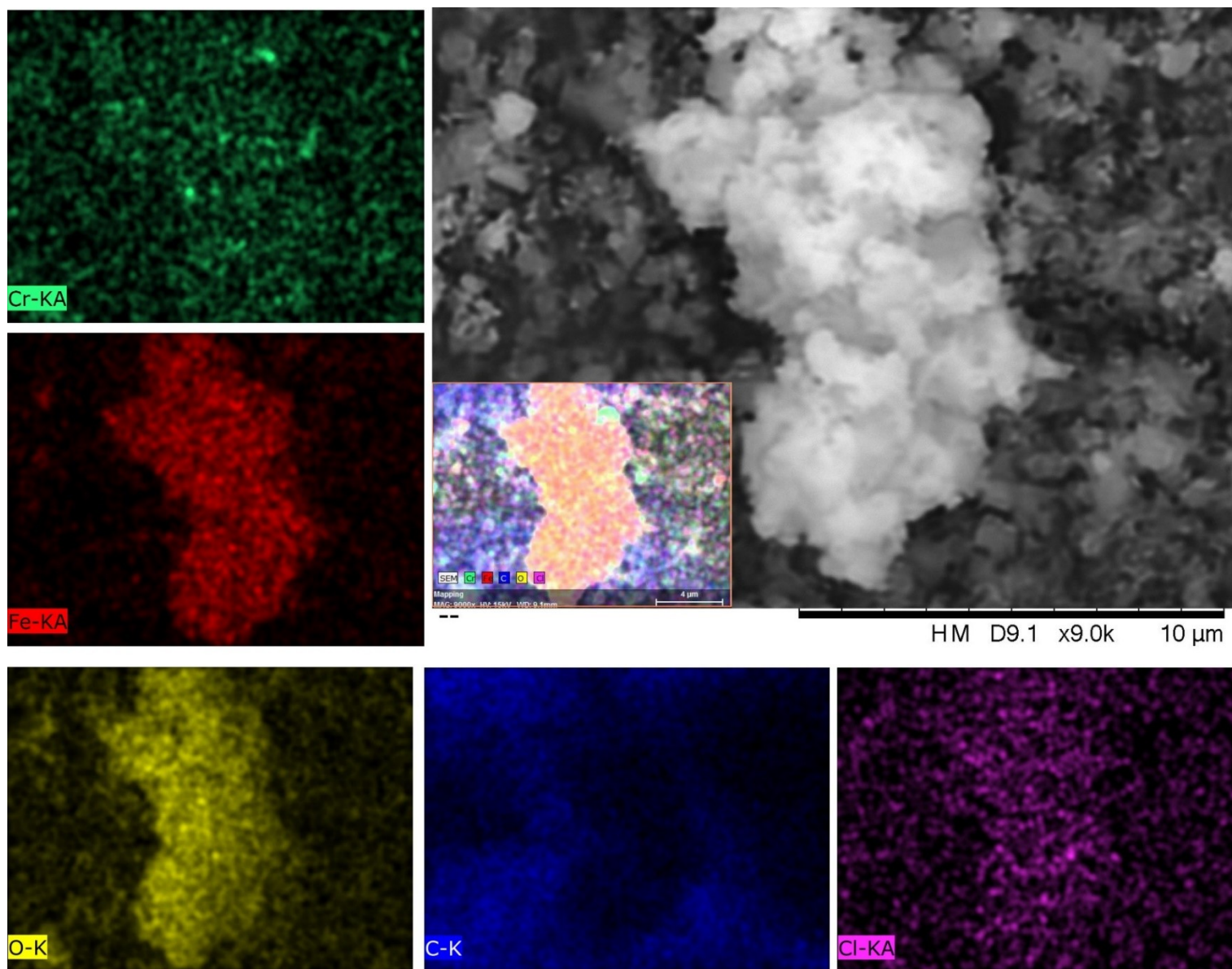


Figure S15. SEM image of the PSM-50-Cl sample with its whole elemental mapping distribution over the sample.

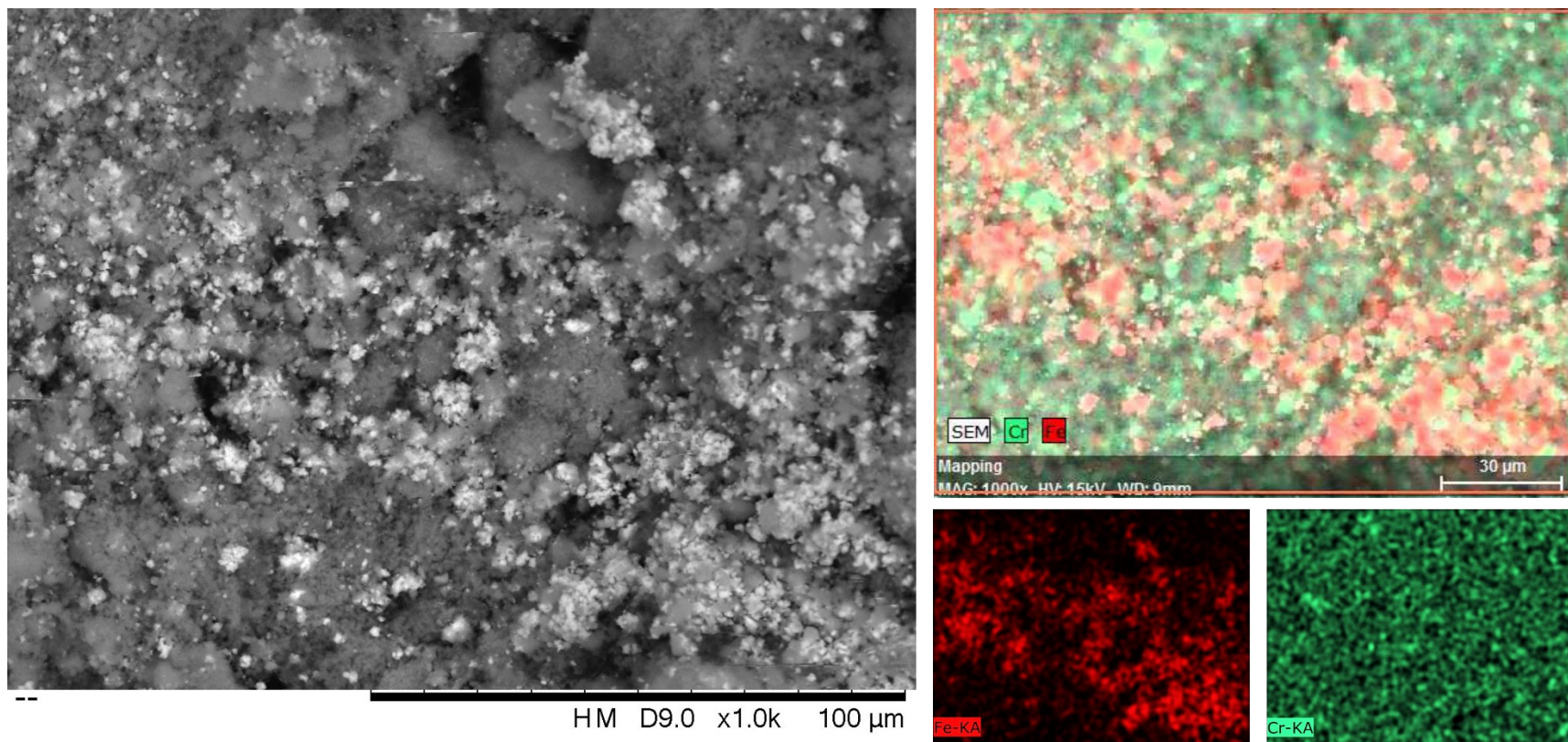


Figure S16. SEM image of the PSM-100-Cl sample with the mapping of the Cr and Fe distribution over the sample.

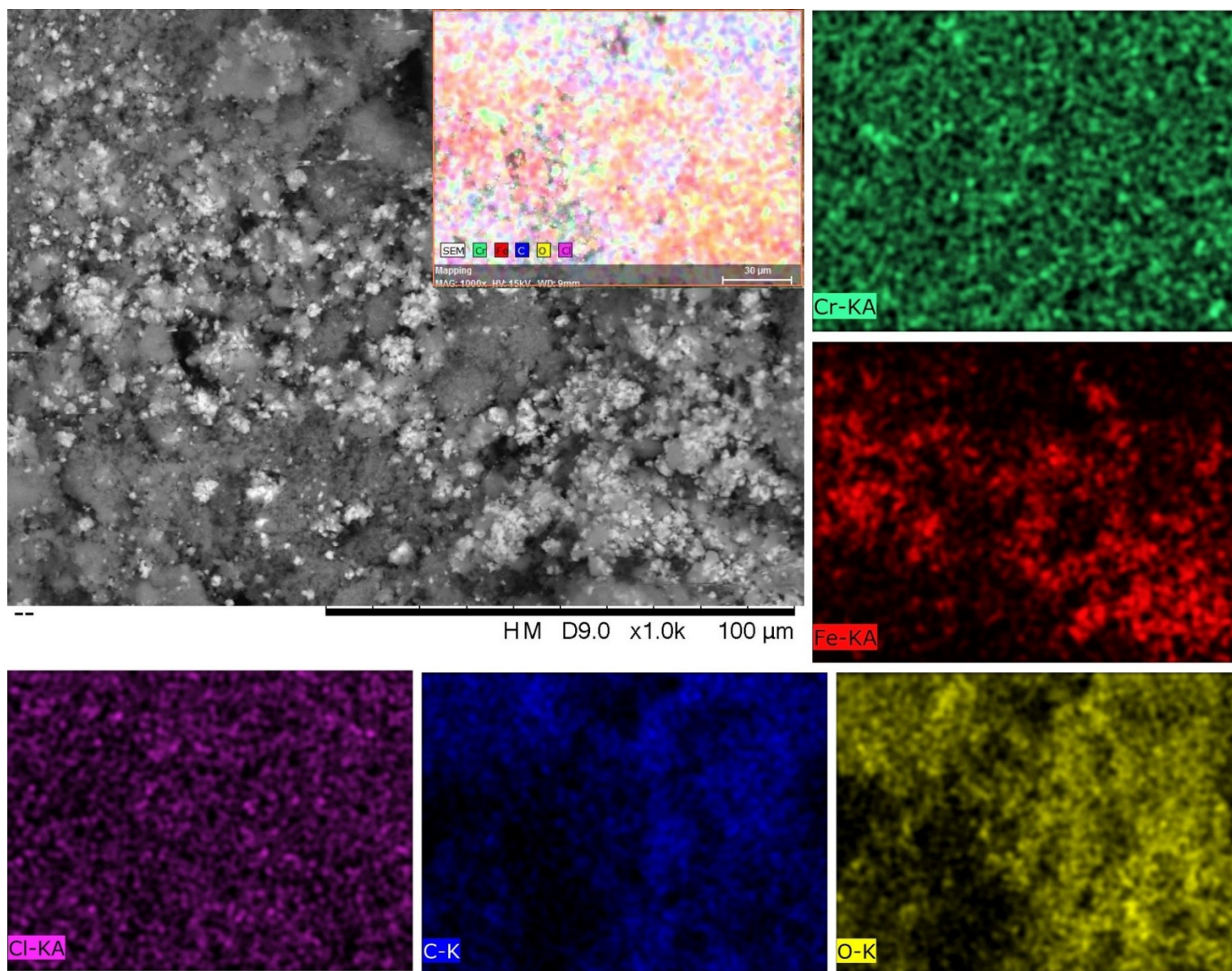


Figure S17. SEM image of the PSM-100-Cl sample with its whole elemental mapping distribution over the sample.

g-BET

Table S9. Specific surface area and pore volume of all PSM samples

Sample	MIL-101(Cr)	PSM-0-Cl	PSM-10-Cl	PSM-25-Cl	PSM-50-Cl	PSM-100-Cl
S_{BET} ($m^2 \cdot g^{-1}$)	2497	2789	2618	2305	2083	2041
$S_{Langmuir}$ ($m^2 \cdot g^{-1}$)	3852	4127	3971	3663	3429	3398
V_{pore}^{\ddagger} ($cm^3 \cdot g^{-1}$)	1.49	1.77	1.60	1.42	1.35	1.32
$V_{pore}^{\ddot{}}$ ($cm^3 \cdot g^{-1}$)	1.14	1.46	1.37	1.11	1.07	1.05
Sample	MIL-101(Cr)	PSM-0-Cl	PSM-10- NO ₃	PSM-25- NO ₃	PSM-50-NO ₃	PSM-100-NO ₃
S_{BET} ($m^2 \cdot g^{-1}$)	2497	2789	2654	2570	2121	2033
$S_{Langmuir}$ ($m^2 \cdot g^{-1}$)	3852	4127	4014	3917	3476	3372
V_{pore}^{\ddagger} ($cm^3 \cdot g^{-1}$)	1.49	1.77	1.62	1.53	1.38	1.31
$V_{pore}^{\ddot{}}$ ($cm^3 \cdot g^{-1}$)	1.14	1.46	1.38	1.27	1.10	1.05
Sample	MIL-101(Cr)	PSM-0-DMF	PSM-10-DMF	PSM-25-DMF	PSM-50-DMF	PSM-100-DMF
S_{BET} ($m^2 \cdot g^{-1}$)	2497	2605	2647	2686	2589	2306
$S_{Langmuir}$ ($m^2 \cdot g^{-1}$)	3852	3959	4006	4058	3950	3667
V_{pore}^{\ddagger} ($cm^3 \cdot g^{-1}$)	1.49	1.52	1.73	1.75	1.51	1.46
$V_{pore}^{\ddot{}}$ ($cm^3 \cdot g^{-1}$)	1.14	1.27	1.40	1.43	1.26	1.12

\ddagger = Barrett-Joyner-Hallender (BJH) method, $\ddot{}$ = Density-functional theory (DFT) method.

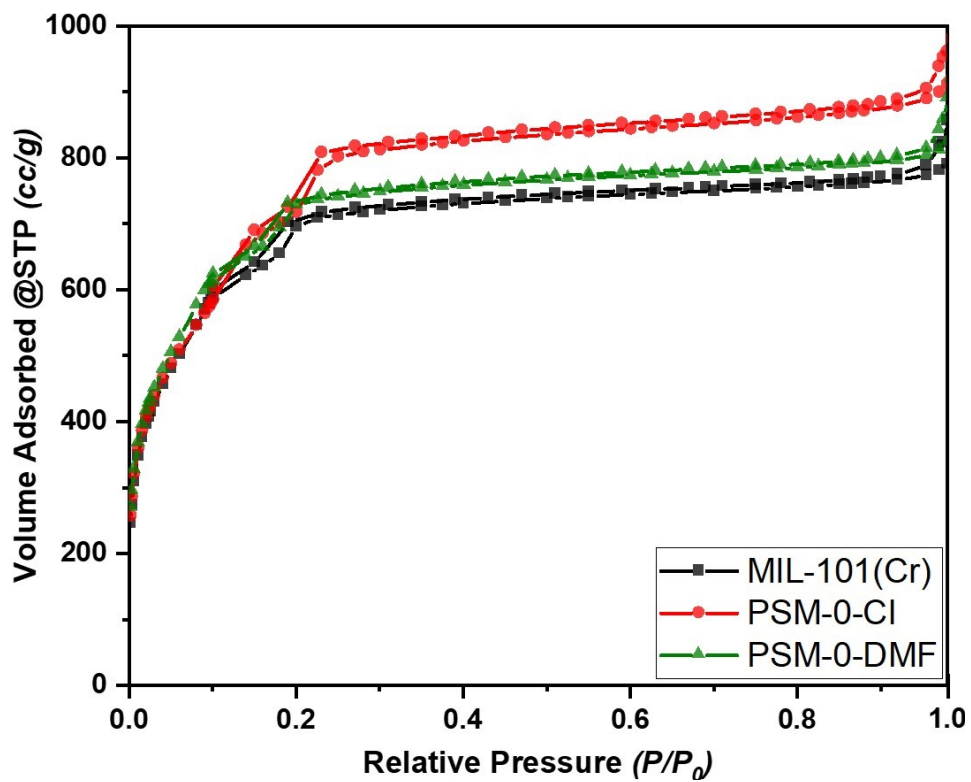


Figure S18. N₂ sorption isotherms for pristine MIL-101(Cr), PSM-10-Cl, and PSM-10-DMF samples.

References

- [1] L. Bromberg, Y. Diao, H. Wu, S. A. Speakman, and T. A. Hatton, "Chromium(III) Terephthalate Metal Organic Framework (MIL-101): HF-Free Synthesis, Structure, Polyoxometalate Composites, and Catalytic Properties," *Chemistry of Materials*, vol. 24, no. 9, pp. 1664-1675, 2012, doi: <https://doi.org/10.1021/cm2034382>.
- [2] M. Ma, A. Bétard, I. Weber, N. S. Al-Hokbany, R. A. Fischer, and N. Metzler-Nolte, "Iron-Based Metal–Organic Frameworks MIL-88B and NH₂-MIL-88B: High Quality Microwave Synthesis and Solvent-Induced Lattice “Breathing”," *Crystal Growth & Design*, vol. 13, no. 6, pp. 2286-2291, 2013, doi: <https://doi.org/10.1021/cg301738p>.
- [3] P. Á. Szilágyi, P. Serra-Crespo, I. Dugulan, J. Gascon, H. Geerlings, and B. Dam, "Post-synthetic cation exchange in the robust metal–organic framework MIL-101(Cr)," *CrystEngComm*, vol. 15, no. 47, pp. 10175-10178, 2013, doi: <https://doi.org/10.1039/C3CE42006J>.
- [4] S. Abednatanzi, P. Gohari Derakhshandeh, H. Depauw, F.-X. Coudert, H. Vrielinck, P. Van Der Voort, and K. Leus, "Mixed-metal metal–organic frameworks," *Chemical Society Reviews*, vol. 48, no. 9, pp. 2535-2565, 2019, doi: <https://doi.org/10.1039/C8CS00337H>.
- [5] R. Fazaeli, H. Aliyan, M. Moghadam, and M. Masoudinia, "Nano-rod catalysts: Building MOF bottles (MIL-101 family as heterogeneous single-site catalysts) around vanadium oxide ships," *Journal of Molecular Catalysis A: Chemical*, vol. 374-375, pp. 46-52, 2013, doi: <https://doi.org/10.1016/j.molcata.2013.03.020>.
- [6] T. A. Vu, G. H. Le, C. D. Dao, L. Q. Dang, K. T. Nguyen, P. T. Dang, H. T. K. Tran, Q. T. Duong, T. V. Nguyen, and G. D. Lee, "Isomorphous substitution of Cr by Fe in MIL-101 framework and its application as a novel heterogeneous photo-Fenton catalyst for reactive dye degradation," *RSC Advances*, vol. 4, no. 78, pp. 41185-41194, 2014, doi: <https://doi.org/10.1039/C4RA06522K>.
- [7] E. Elsayed, P. Anderson, R. Al-Dadah, S. Mahmoud, and A. Elsayed, "MIL-101(Cr)/calcium chloride composites for enhanced adsorption cooling and water desalination," *Journal of Solid State Chemistry*, vol. 277, pp. 123-132, 2019, doi: <https://doi.org/10.1016/j.jssc.2019.05.026>.
- [8] H. Su, J. Lv, L. Yang, L. Feng, Y. Liu, Z. Du, and L. Zhang, "Rapid and selective adsorption of a typical aromatic organophosphorus flame retardant on MIL-101-based metal–organic frameworks," *RSC Advances*, vol. 10, no. 4, pp. 2198-2208, 2020, doi: <https://doi.org/10.1039/C9RA09062B>.
- [9] M. Lammert, S. Bernt, F. Vermoortele, D. E. De Vos, and N. Stock, "Single- and Mixed-Linker Cr-MIL-101 Derivatives: A High-Throughput Investigation," *Inorganic Chemistry*, vol. 52, no. 15, pp. 8521-8528, 2013, doi: <https://doi.org/10.1021/ic4005328>.
- [10] M. Sheikh Alivand, N. H. M. Hossein Tehrani, M. Shafiei-alavijeh, A. Rashidi, M. Kooti, A. Pourreza, and S. Fakhraie, "Synthesis of a modified HF-free MIL-101(Cr) nanoadsorbent with enhanced H₂S/CH₄, CO₂/CH₄, and CO₂/N₂ selectivity," *Journal of Environmental Chemical Engineering*, vol. 7, no. 2, p. 102946, 2019, doi: <https://doi.org/10.1016/j.jece.2019.102946>.
- [11] M. Asiabi, A. Mehdinia, and A. Jabbari, "Electrospun biocompatible Chitosan/MIL-101 (Fe) composite nanofibers for solid-phase extraction of Δ 9-tetrahydrocannabinol in whole blood samples using Box-Behnken experimental design," *Journal of Chromatography A*, vol. 1479, pp. 71-80, 2017, doi: <https://doi.org/10.1016/j.chroma.2016.12.024>.
- [12] Y. Liu, Y. Xie, M. Dai, Q. Gong, and Z. Dang, "Ag/AgCl/MIL-101(Fe) Catalyzed Degradation of Methylene Blue under Visible Light Irradiation," *Materials*, vol. 12, no. 9, p. 1453, 2019, doi: <https://doi.org/10.3390/ma12091453>.